and Taniguchi, N. (2001) *J Biol Chem* **276**(35), 32867-32874

37. Hoffmeister, K. M., Josefsson, E. C., Isaac, N. A., Clausen, H., Hartwig, J. H., and Stossel, T. P. (2003) *Science* **301**(5639), 1531-1534
38. Josefsson, E. C., Gebhard, H. H., Stossel, T. P., Hartwig, J. H., and Hoffmeister, K. M. (2005) *J Biol Chem* **280**(18), 18025-18032
39. Endo, T., and Manya, H. (2006) *Methods Enzymol* **417**, 137-152
40. Manya, H., Chiba, A., Yoshida, A., Wang, X., Chiba, Y., Jigami, Y., Margolis, R. U., and Endo, T. (2004) *Proc Natl Acad Sci U S A* **101**(2), 500-505
41. Manya, H., Suzuki, T., Akasaka-Manya, K., Ishida, H. K., Mizuno, M., Suzuki, Y., Inazu, T., Dohmae, N., and Endo, T. (2007) *J Biol Chem* **282**(28), 20200-20206
42. Ju, T., and Cummings, R. D. (2002) *Proc Natl Acad Sci U S A* **99**(26), 16613-16618
43. Ju, T., and Cummings, R. D. (2005) *Nature* **437**(7063), 1252
44. Sasai, K., Ikeda, Y., Ihara, H., Honke, K., and Taniguchi, N. (2003) *J Biol Chem* **278**(28), 25295-25301

FOOTNOTES

*This work was partly supported by Core Research for Evolutional Science and Technology (CREST), the Japan Science and Technology Agency (JST) and the "Academic Frontier" Project for Private Universities from the Ministry of Education, Culture, Sports, Science and Technology of Japan, and Takeda Science Foundation, Japan.

The abbreviations used in this paper are as follow: BSA, bovine serum albumin; DSA, Datura stramonium; E_4-PHA, erythroagglutinating phytohemagglutinin; FACS, fluorescence activated cell sorting; FCS, fetal calf serum; FN, fibronectin; GFP, green fluorescent protein; GlcNAc, *N*-acetylglucosamine; GnT-III, N-acetylglucosaminyltransferase III; GnT-V, *N*-acetylglucosaminyltransferase V; L_4-PHA, leukoagglutinating phytohemagglutinin; PBS, phosphate-buffered saline. TBS, Tris-buffered saline.

FIGURE LEGENDS

Fig. 1. Potential *N*-glycosylation sites on the α5 subunit and its modification by GnT-III and GnT-V. (*A*) Schematic diagram of potential *N*-glycosylation sites on the α5 subunit. Putative *N*-glycosylation sites are indicated by the triangles, and point mutations are indicated by crosses (N84Q, N182Q, N297Q, N307Q, N316Q, N524Q, N530Q, N593Q, N609Q, N675Q, N712Q, N724Q, N773Q, and N868Q). (*B*) Illustration of the reaction catalyzed by GnT-III and GnT-V. Square, GlcNAc; circle, mannose.

Fig. 2. Comparison of *N*-glycosylation patterns on α5 subunits modified by GnT-III and GnT-V. GnT-III and GnT-V expression vectors were transfected into S-3,4,5 cells using the Phoenix retrovirus system, and stable expression cells were established as described in the "Experimental Procedures." Confluent cells were harvested and lysed for immunoblotting. Equal amounts of protein (20 μg) were separated on 7.5% SDS-PAGE under reducing conditions and the membranes were probed with antibodies against GnT-III (*A, upper panel*) and GnT-V (*B, upper panel*), or with the E4-PHA (*A, middle panels)* and L4-PHA lectins (*B, middle panels*), and reprobed with anti-α-tubulin, which was used as loading control (*A and B, lower panels*). Asterisks indicate nonspecific staining for E4-PHA or L4-PHA. (*C*), Cell lysates were subjected to immunoprecipitation using agarose-conjugated anti-GFP antibody. The immunoprecipitates were subjected to 6.0% SDS-PAGE under non-reducing conditions, blotted and probed with E4-PHA, L4-PHA, and DSA lectins, or probed with antibody against the α5 subunit.

Fig. 3. Effects of overexpression of GnT-III and GnT-V on FN-mediated cell adhesion and migration in S-3,4,5 mutants. (*A*), Subconfluent cells were detached and 40,000 cells were added to the 96-well plates coated with 3 μg/ml of FN for the cell adhesion assay. The plates were incubated at 37 °C for 20 min, then washed twice with warmed PBS(-) to remove non-adherent cells. The adherent cells were fixed with 25% glutaraldehyde, stained with 0.5 % crystal violet and then the absorbance at 590 nm was measured. The bars represent the standard deviation. (*B*), Cell adhesion kinetics assay using RT-CES system. Subconfluent cells were detached and 10,000 cells were applied to wells of an E-Plate coated with 10 μg/ml of FN. The device was operated with RT-CES SP software. The cell index represents the extent of cell adhesion. The bars represent the standard deviation. (*C*), Cell migration toward FN was determined using the transwell assay as described in the "Experimental Procedures." Cells that migrated were stained with 0.5% crystal violet and counted under a microscope. The bars represent the standard deviation. A representative example is shown in the right panel. (*D*), Subconfluent cells were detached and labeled with primary antibody (mouse anti-human VLA5 antibody, HA5) for 30 min on ice. The labeled cells were washed with ice-cold PBS, and then incubated with Alexa Fluor 647 goat anti-mouse IgG for 30 min on ice. The expression levels of α5 integrin on the cell surface were measured using FACS Calibur instrument (BD Biosciences). Negative controls were not treated with the primary antibody, but underwent all other procedures.

Fig. 4. Comparison of effects of GnT-III on *N*-glycosylation and cell adhesion between S-3,5 and S-4,5 mutants. (*A*), GnT-III was expressed in S-3,5 and S-4,5 mutants, and stable

expression cells were established as described in the "Experimental Procedures." The expression levels of GnT-III were detected with an antibody against GnT-III. (*B*), Confluent cells were lysed and then subjected to immunoprecipitaion using an agarose-conjugated antibody against GFP. The immunoprecipitates were subjected to 6.0% SDS-PAGE under non-reducing conditions, blotted and probed with E4-PHA (right panel), then reprobed with antibody against the α5 subunit (left panel). (*C*), The cell adhesion assay was carried out as described above (Fig. 3A). The bars represent the standard deviation. (*D*), The cell adhesion kinetics assay using the RT-CES system was the same as that described in Fig.3B. Subconfluent cells were detached and 40,000 cells were added to the wells. The cell index reflects the extent of cell adhesion. The bars represent the standard deviation. (*E*), The S-3,5 and S-4,5 expression vectors were transfected into Hela cells using the Phoenix retrovirus system, and selected with puromycin as described in the "Experimental Procedures." The cells were lysed, and the amounts of cell lysate (2 mg) were then subjected to immunoprecipitaion using an agarose-conjugated antibody against GFP. The immunoprecipitates were subjected to 6.0% SDS-PAGE under non-reducing conditions, blotted and probed with E4-PHA (upper panel), then reprobed with antibody against the α5 subunit (lower panel).

Fig. 5. Comparison of GnT-III modification among wild-type (WT), site-3 (D-3) and site-4 (D-4) deletion mutants. GnT-III was expressed in WT, D-3 and D-4 deletion mutants, and stable expression cells were established as described in the "Experimental Procedures." The expression levels of the GnT-III and GnT-III products in total cell lysates were detected with antibodies against GnT-III (*A, upper panel*) and α-tubulin to ensure equal loading (*A, lower panel*), respectively. (*B*), The cell lysates were subjected to immunoprecipitaion using an agarose-conjugated antibody against GFP. The immunoprecipitates were separated on 6.0% SDS-PAGE under non-reducing conditions. The membrane blot was probed with E4-PHA lectin, and then was reprobed with an antibody against the α5 subunit. The ratio of E4-PHA to total α5 staining in WT cells was set equal to 1.0. (*C*), the percentages of spread cells were quantified and expressed as the mean ± S.D. from three independent experiments. The rounded cells were not considered as spread cells. The ratio of spread cells versus total cells (~300 cells) of WT transfectants was set as 100.

Fig.1. Sato, Y., et al

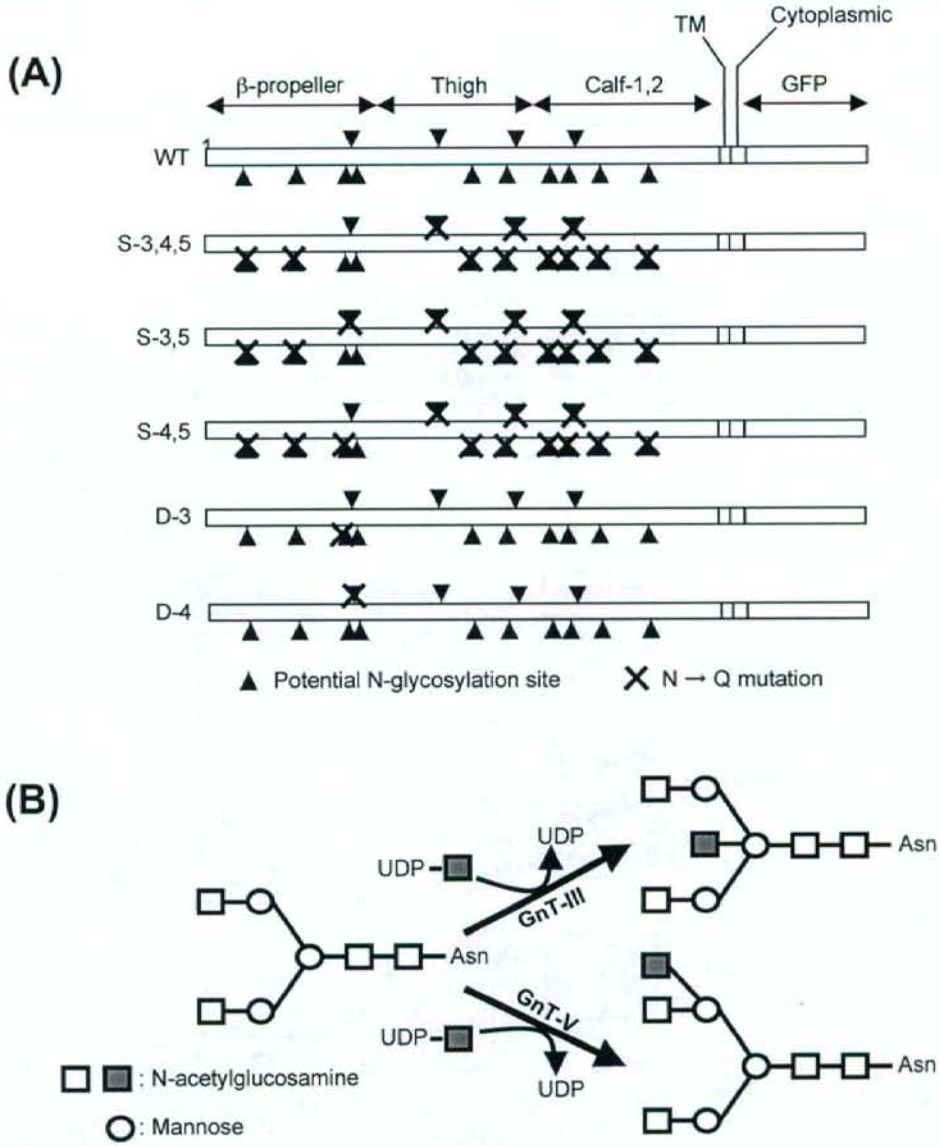

Fig.2. Sato, Y., et al

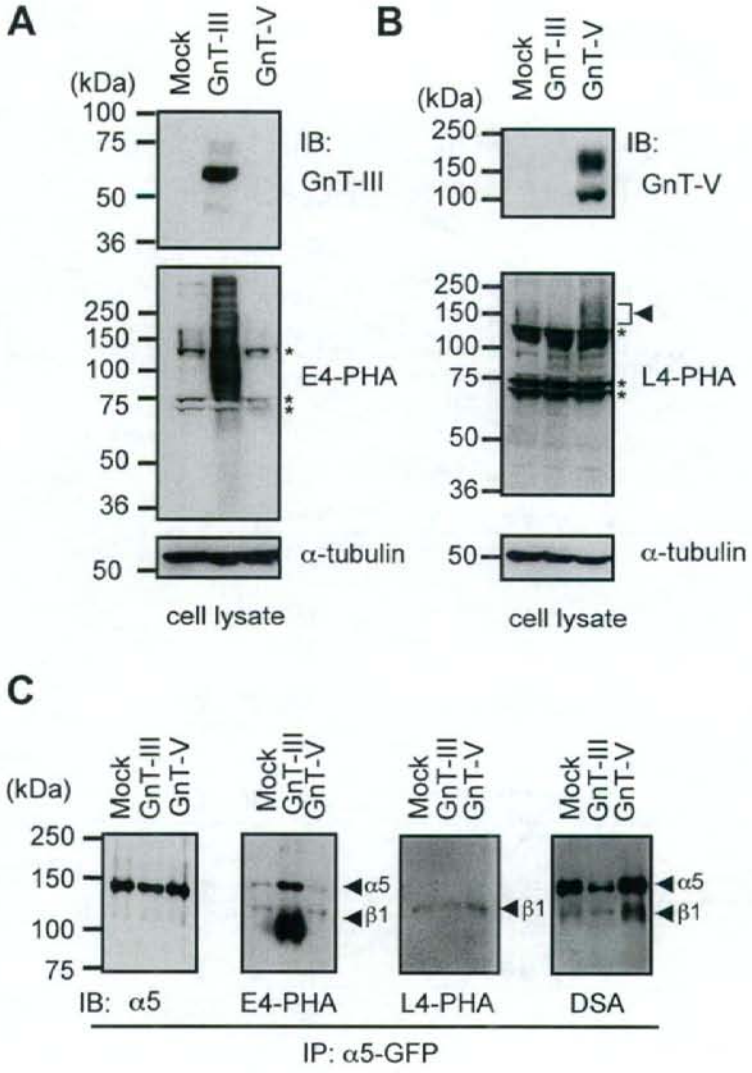

Fig.3a. Sato, Y., et al

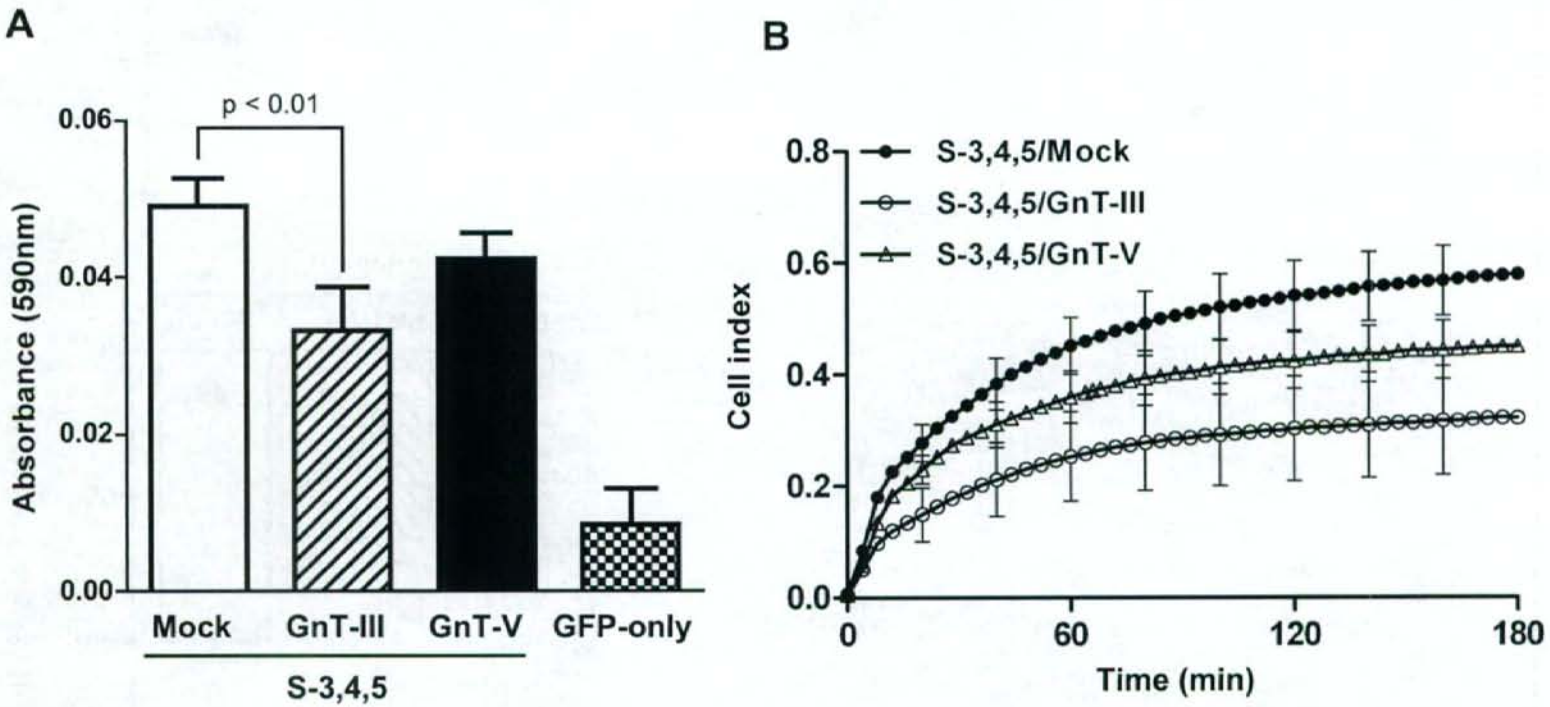

Fig.3b. Sato, Y., et al

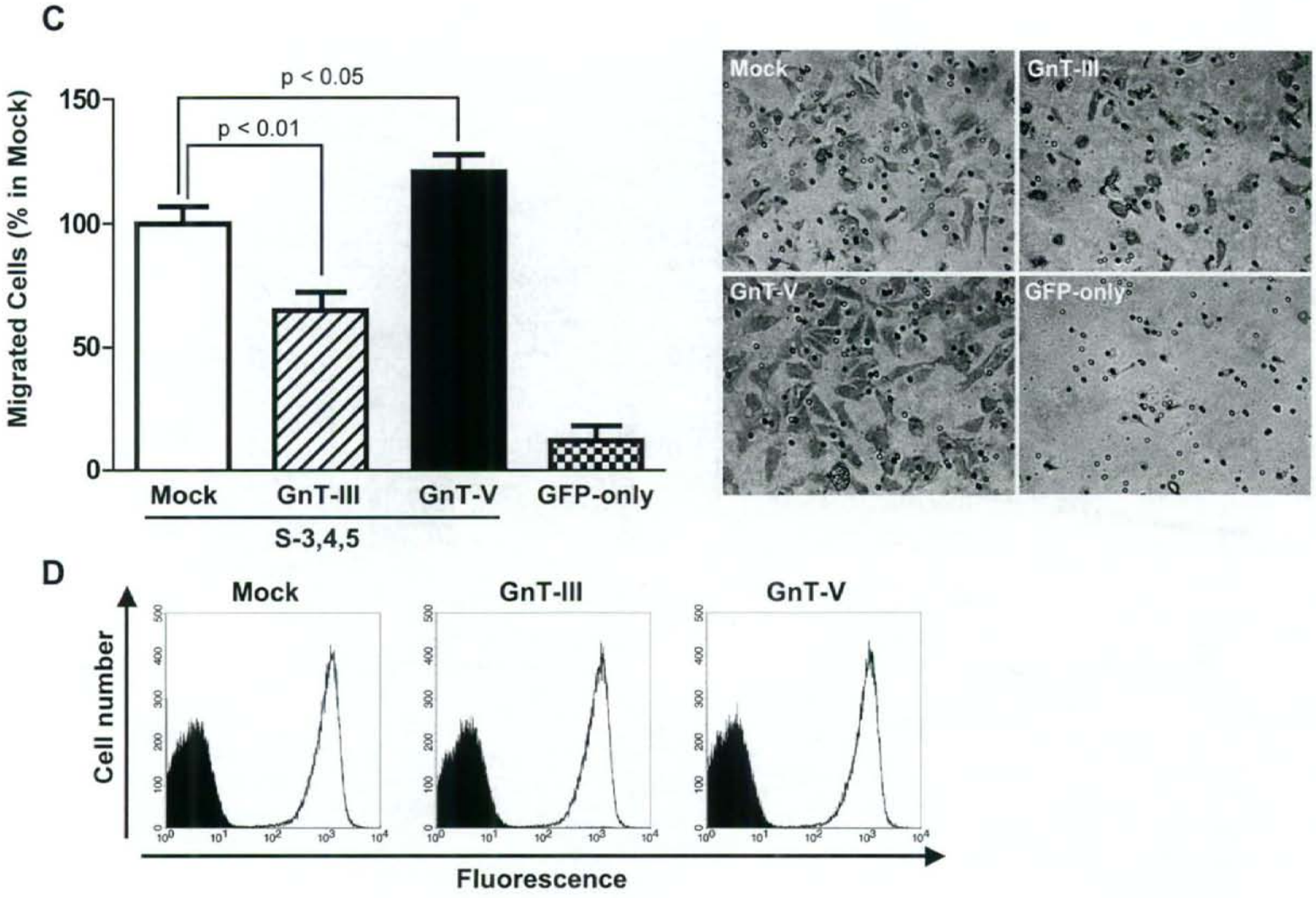

Fig.4. Sato, Y., et al

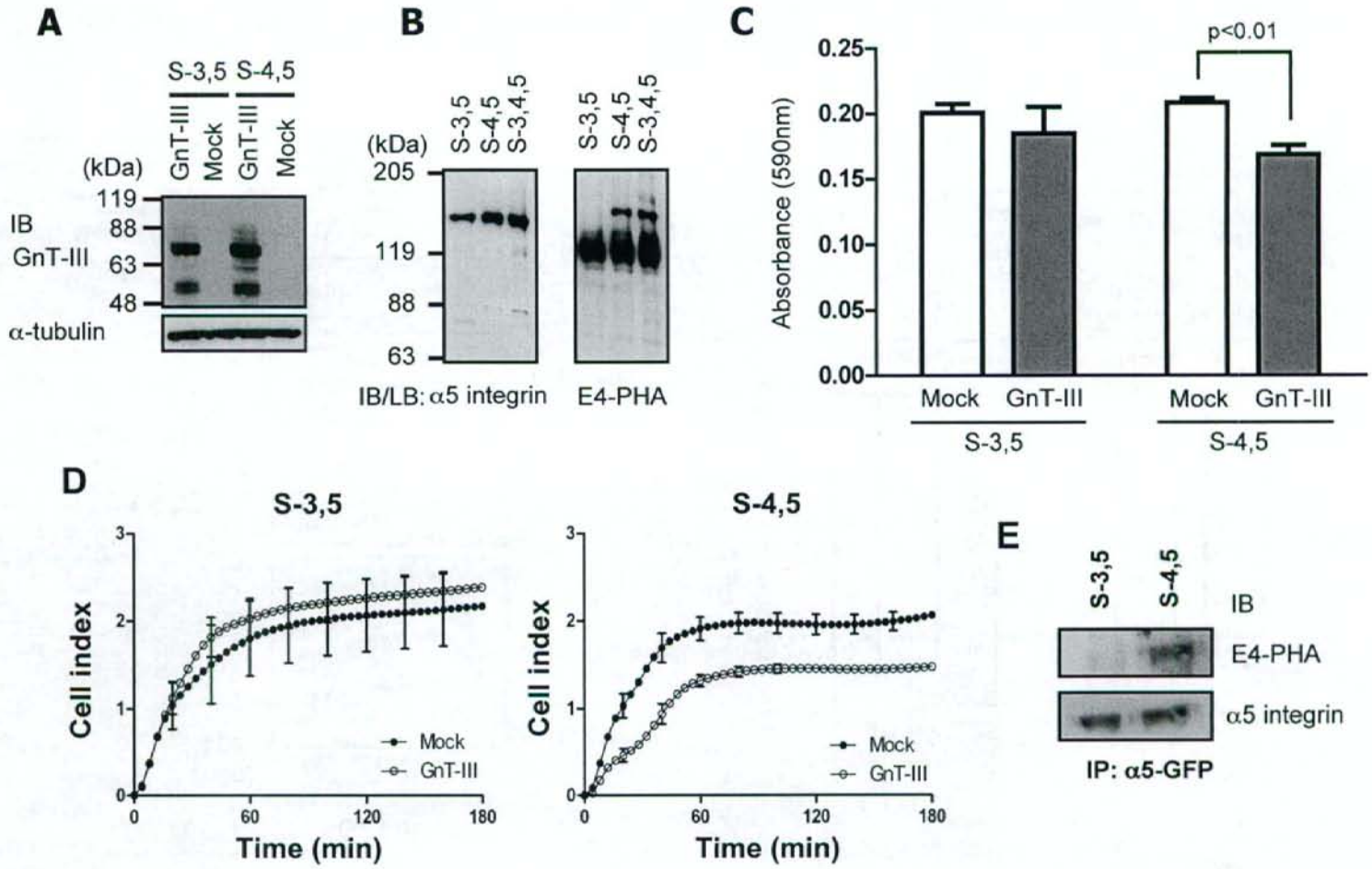

Fig.5. Sato, Y., et al

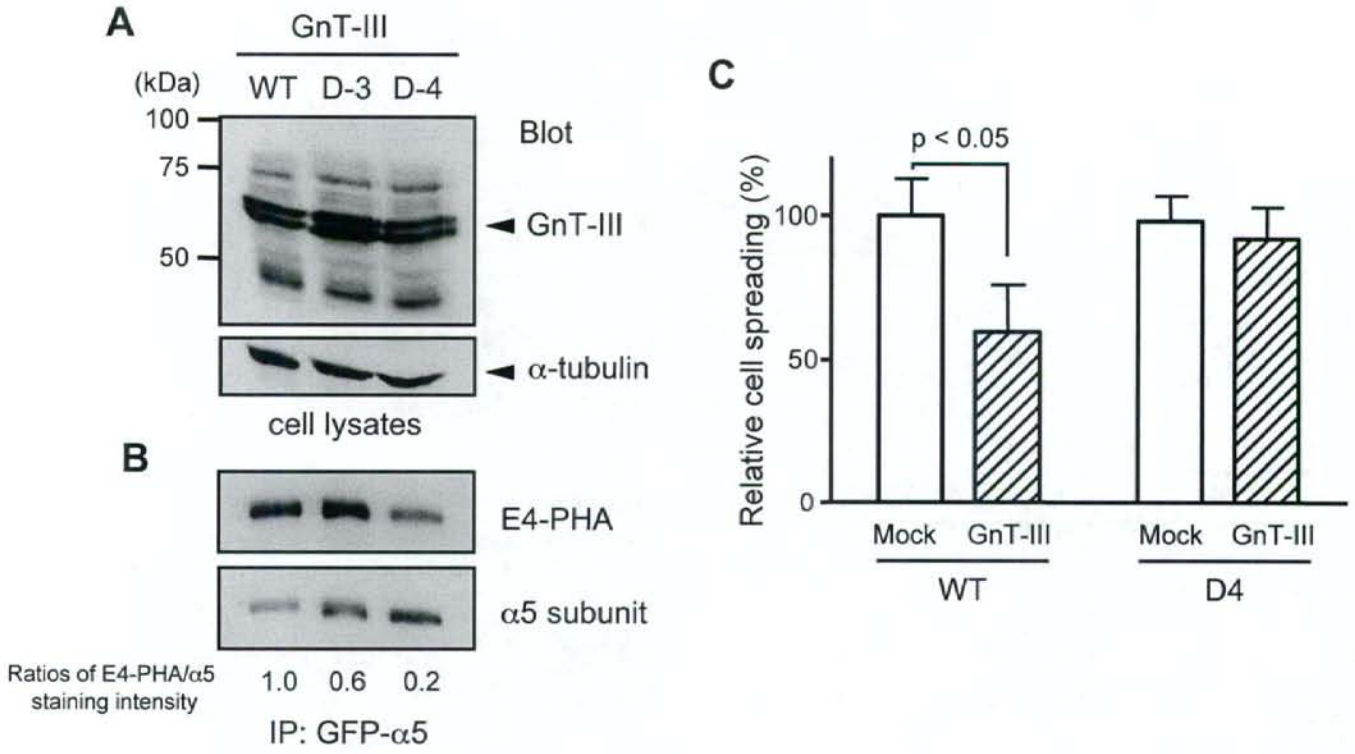

Epilysin (MMP-28) Restrains Early Macrophage Recruitment in *Pseudomonas aeruginosa* Pneumonia[1]

Anne M. Manicone,[2*†] Timothy P. Birkland,[*†] Michelle Lin,[*†] Tomoko Betsuyaku,[‡] Nico van Rooijen,[§] Jouko Lohi,[¶] Jorma Keski-Oja,[¶] Ying Wang,[*†] Shawn J. Skerrett,[†] and William C. Parks[*†]

Several members of the matrix metalloproteinase (MMP) family function in various processes of innate immunity, particularly in controlling leukocyte influx. Epilysin (MMP-28) is expressed in numerous tissues and, in adult mice, it has the highest expression in lung, where it is detected in bronchial epithelial cells (Clara cells). Epilysin is also expressed by bone marrow-derived macrophages, but not by alveolar macrophages, suggesting that its expression by macrophages is dependent on localization and differentiation. To assess the role of this MMP, we generated epilysin-null (*Mmp28*$^{-/-}$) mice. Although epilysin is constitutively expressed in normal tissues, *Mmp28*$^{-/-}$ mice have no overt phenotype. However, using a murine model of *Pseudomonas aeruginosa* pneumonia, we found that *Mmp28*$^{-/-}$ mice had an early increase in macrophage recruitment into the lungs, as well as enhanced bacterial clearance and reduced pulmonary neutrophilia, which we predicted were due to accelerated macrophage influx. Macrophage depletion in WT and *Mmp28*$^{-/-}$ mice confirmed a role for macrophages in clearing *P. aeruginosa* and regulating neutrophil recruitment. Furthermore, we observed that macrophages derived from *Mmp28*$^{-/-}$ mice migrated faster than did wild-type cells to bronchoalveolar lavage fluid from *P. aeruginosa*-treated mice of either genotype. These observations indicate that epilysin functions as an intrinsic negative regulator of macrophage recruitment by retarding the chemotaxis of these cells. *The Journal of Immunology*, 2009, 182: 3866–3876.

The innate immune system evolved as a rapid response to defend against pathogens and includes ready-to-go bactericidal and proinflammatory processes and the activities of both resident cells and infiltrating leukocytes (1). As the barrier separating the environment from internal tissues, epithelia are key effectors that respond to challenge and control various immune processes (2). For example, in response to infection or injury, epithelial cells produce various proteins and other factors that govern (both promote and restrain) the influx of inflammatory cells, particularly neutrophils and macrophages. Macrophages, which comprise a diverse group of cells, are critical effector cells that bridge innate and adaptive immune responses (3). Both resident macrophages and infiltrated monocytes can directly kill bacteria and, via their ability to release a range of bioactive factors, such as chemokines, TNF-α, and more, shape both the pattern and duration of an acute inflammatory reaction (4). Additionally, as professional APCs, macrophages are essential effectors of lymphocytic responses linking innate and adaptive immunity. Thus, identifying the products and pathways that control macrophage recruitment and activity is central to a clearer understanding of immune functions.

Matrix metalloproteinases (MMPs)[3] have emerged as key effector enzymes regulating distinct stages of inflammation, and recent insights from in vitro and mouse models of human disease indicate that MMPs evolved to serve important functions in innate immunity (5, 6). The expression of MMPs in injured or inflamed tissues has led to the general concept that these proteinases mediate proinflammatory functions. Indeed, several MMPs promote leukocyte influx by modulating cytokine or chemokine activity (5–13). For example, work done in our laboratory demonstrated that matrilysin (MMP-7) promotes neutrophil efflux across an epithelial barrier via shedding the transmembrane proteoglycan syndecan-1 complexed with KC, a murine CXC chemokine (9). Collagenase-2 (MMP-8) processes the CXC chemokine LIX to a more active form, predicting that it functions to stimulate neutrophil influx (14). Similarly, gelatinases A (MMP-2) and B (MMP-9) regulate the trafficking of specific inflammatory cells from the peribronchovascular bundle into the alveolar space via affecting the formation of CC chemokine gradients (8, 15).

Epilysin (MMP-28), the newest and apparently last member of the mammalian MMP family, was cloned in our laboratory from human keratinocyte and testis cDNA libraries (16, 17). Like other MMPs, epilysin contains a prodomain, a zinc-binding catalytic domain, and a hemopexin-like domain. Additionally, epilysin contains a furin activation sequence and, hence, it is activated within the secretion pathway by cleavage of its prodomain (18). In human tissue, epilysin mRNA is expressed at high levels in the testis, lung, heart, GI tract, and in wounded epidermis (18). In mice, epilysin mRNA is produced in placenta, heart, uterus, testis,

*Center for Lung Biology and †Division of Pulmonary and Critical Care Medicine, University of Washington, Seattle, WA 98109; ‡First Department of Medicine, Hokkaido University, Sapporo, Japan; §Department of Cell Biology, Faculty of Medicine, Free University, Amsterdam, The Netherlands; and ¶Department of Pathology, University of Helsinki and Helsinki University Central Hospital, Helsinki, Finland

Received for publication December 24, 2007. Accepted for publication January 16, 2009.

The costs of publication of this article were defrayed in part by the payment of page charges. This article must therefore be hereby marked *advertisement* in accordance with 18 U.S.C. Section 1734 solely to indicate this fact.

[1] This work was supported by National Institutes of Health Grants HL077555 and HL084385 and by the Academy of Finland and Helsinki University Hospital.

[2] Address correspondence and reprint requests to Dr. Anne M. Manicone, Center for Lung Biology, University of Washington, 815 Mercer Street, Seattle, WA 98109. E-mail address: manicone@u.washington.edu

[3] Abbreviations used in this paper: MMP, matrix metalloproteinase; BALF, bronchoalveolar lavage fluid; BMDM, bone marrow-derived macrophage; CCSP, Clara cell secretory protein; ES, embryonic stem; LCM, laser capture microdissection; qRT-PCR, quantitative RT-PCR; WT, wild type.

www.jimmunol.org/cgi/doi/10.4049/jimmunol.0713949

gastrointestinal tract, and lung, which has the highest level of expression. In tissue and cell cultures, epilysin is predominantly expressed by epithelium, including keratinocytes, placental villi, and airway epithelial cells (16, 18, 19). In addition to its predominant expression by epithelium, bone marrow-derived macrophages (BMDM) also express epilysin.

Because several MMPs function in immunity, we hypothesized that epilysin may have a regulatory role in the tissue response to environmental challenge. To test this, we generated epilysin-null mice ($Mmp28^{-/-}$). Similar to many other MMP-null mice, $Mmp28^{-/-}$ mice revealed no overt phenotype. However, as we report herein, when challenged with *Pseudomonas aeruginosa*, a relevant respiratory pathogen, $Mmp28^{-/-}$ mice had accelerated macrophage recruitment compared with wild-type (WT) mice. Additionally, these knockout mice had enhanced bacterial clearance and reduced pulmonary neutrophilia, which we predict are two potential consequences of enhanced macrophage influx. Macrophage depletion in WT and $Mmp28^{-/-}$ mice confirmed a role for macrophages in clearing *P. aeruginosa* and regulating neutrophil recruitment. Furthermore, we observed that BMDM, which express epilysin, migrate at a slower rate when compared with BMDM cultured from $Mmp28^{-/-}$ mice. These observations indicate that epilysin functions as an intrinsic negative regulator of macrophage recruitment by retarding the chemotaxis of macrophages.

Materials and Methods

Mice

We cloned the mouse *Mmp28* gene from the SV129 genome (gene ID 118453) (20). To construct the homologous extensions of the targeting construct, we isolated a 4.8-kb *Eco*RI-*Xba*I fragment containing the 3′ terminus of intron 1, exons 2 and 3, and ~4 kb of intron 3 and a 2.1-kb *Xho*I-*Eco*RI fragment containing the 3′ untranslated end of exon 8 and downstream sequence (Fig. 1*A*). A pgk-neomycin resistance cassette was inserted between the two arms and a diphtheria toxin (dta) cassette was ligated to the 3′ end. The targeting construct was linearized with *Xho*I (the *Xho*I site at the 5′ end of the short arm was deleted by ligating to the *Sal*I site in the neomycin cassette).

Transfection of 129X1/SvJ (RW4) embryonic stem (ES) cells was done by the Murine Embryonic Stem Cell Core of the Siteman Cancer Center at Washington University (St. Louis, MO). To screen ES cell clones, genomic DNA was isolated and digested with *Bam*HI. Southern blotting of the digests was done using a 694-bp probe to the 3′ terminal end of intron 1, upstream of the targeting construct (Fig. 1*A*). Selected ES cells were injected into C57BL/6 blastocysts by the Mouse Models Core at Washington University. Genotyping of mouse tail DNA was done by PCR and confirmed by Southern hybridization (Fig. 1*B*). For PCR, we used two forward primers, one specific to the WT locus (5′GTGAAGATGTCCCATGCCCA CAGT3′) and the other to the target construct (5′GAGGAAATTGCATCG CATTGTCTGAG3′), and a common reverse primer (5′CACATTCCCTC CTGCTCTGCATCC3′) to generate a 259 nt product from the WT epilysin gene and a 324 nt product from the mutated gene (Fig. 1*C*). Male chimeric mice were bred to female C57BL/6 mice to generate germline heterozygotes, which were then bred to yield homozygous nulls. $Mmp28^{+/-}$ mice were then backcrossed for 10 generations with C57BL/6 mice from Taconic. Wild-type and $Mmp28^{-/-}$ mice (C57BL/6NTac background) were housed in microisolator cages under specific pathogen-free conditions. Animal experiments were approved by the Institutional Animal Care and Use Committees at Washington University and at the University of Washington (Seattle, WA). Litter-matched mice of both genotypes were used for all studies.

Exposure models

P. aeruginosa strain PAK, a nonmucoid, flagellated strain originally obtained from Dr. Stephen Lory (Harvard University), was grown in Luria-Bertani broth at 37°C, collected and counted during stationary phase, and suspended in 20 ml of PBS. Mice were exposed to bacterial aerosols generated by twin jet nebulizers (Salter Labs) for 30 min in a whole animal chamber to achieve a high dose deposition of 10^5-10^6 bacteria/lung as described (21). To assess initial bacterial deposition, four mice (two of each genotype) were sacrificed immediately after aerosolization for quantitative culture of whole-lung homogenates. The remaining mice ($n = 10$ mice/time point) were sacrificed at 4 and 24 h. The left lung was homogenized in PBS for quantitative bacterial culture. The remaining lung homogenate was diluted 1/1 in lysis buffer containing 2× protease inhibitor cocktail (Roche Diagnostics), incubated on ice for 30 min, and centrifuged at 1500 × *g*. The supernatant was stored at −80°C for cytokine levels. The right lung was lavaged for determination of cell counts and differential and total protein and chemokine/cytokine levels. Postlavage, the right lung was inflated to 15 cm H_2O with 4% paraformaldehyde and embedded in paraffin. In separate experiments, the left lung was collected and homogenized in TRIzol B (Invitrogen) for RNA extraction per the manufacturer's protocol. To assess bacteremia, spleens were harvested and homogenized in PBS for quantitative bacterial culture.

In macrophage depletion experiments, *P. aeruginosa* strain PAK was administered via intranasal inoculation using 1×10^7 organisms/lung. Bacteria were grown overnight in Luria-Bertani broth at 37°C, collected, and quantified during the stationary phase. Bacteria were resuspended in PBS, and 50 μl was administered via intranasal inoculation in mice sedated with 425 mg/kg Avertin (2,2,2-tribromothanol).

Macrophage depletion

The clodronate-encapsulated liposomes and PBS-encapsulated liposomes were prepared as described (22). Clodronate was a gift of Roche Diagnostics. Phosphatidylcholine was obtained from Lipoid, and cholesterol was purchased from Sigma-Aldrich. Clodronate-encapsulated liposomes were delivered both intranasally (50 μl) and i.p. (200 μl) to deplete alveolar macrophages and circulating monocytes, respectively. PBS-encapsulated liposomes were delivered in a similar fashion as a control. Forty-eight hours after treatment, two to four mice in each group were harvested to determine efficacy of macrophage and monocyte depletion by performing cell counts and differential of bronchoalveolar lavage fluid (BALF) and buffy coats. In a separate set of experiments, mice (macrophage-depleted and undepleted WT and $Mmp28^{-/-}$ mice, 10 mice/group) received intranasal instillation of 10^7 *P. aeruginosa* PAK strain. These mice were then harvested at 4 and 24 h for BALF cell counts, differential, histology, and bacterial counts.

Laser capture microdissection (LCM)

At 24 or 72 h after LPS instillation, mice were sacrificed and lungs were inflated with diluted Tissue-Tek OCT (Sakura Finetek), 50% (v/v) in RNase-free PBS containing 10% sucrose, and immediately frozen on dry ice as described (23). Tissue sections (7 μm) were processed and stained as described in detail (23). LCM was done to retrieve cells within 100 μm of the bronchoalveolar junction using the PixCell II system (Arcturus Engineering) with the following parameters: laser diameter, 30 μm; pulse duration, 5 ms; and amplitude, 50 mW, as described previously (23, 24). Approximately 10,000 laser bursts were used to collect cells from each mouse. After the samples were captured on transfer films (CapSure Macro LCM caps, LCM0211; Arcturus Engineering), nonspecific attached components were removed using adhesive tape (CapSure cleanup pad, LCM0206; Arcturus Engineering).

Quantitative RT-PCR (qRT-PCR)

Total RNA from lung was isolated with TRIzol (Invitrogen) and from LCM-retrieved bronchiolar epithelial cells using an RNeasy Mini kit (Qiagen). The quantity and quality of RNA were determined using an RNA LabChip kit (Agilent Technologies) or a NanoDrop spectrophotometer. Primers and TaqMan probes (FAM dye-labeled) for MMP-7, -10, -12, -14, and -28, Clara cell secretory protein (CCSP), β_2-microglobulin, hypoxanthine phosphoribosyltransferase, or GAPDH were added to cDNA synthesized from 5 μg of total RNA with a High-Capacity cDNA Archive kit (Applied Biosystems), and product amplification was measured with an ABI HT7900 Fast real-time PCR system. The threshold cycle (*Ct*) was obtained from duplicate samples and averaged. The ΔCt was the difference between the average *Ct* for the specific cDNAs. The $\Delta\Delta Ct$ was the average ΔCt at a given time point minus the average ΔCt of day 0 (uninfected) samples. The data are expressed as relative quantification, which is the fold change and is calculated as $2^{-\Delta\Delta Ct}$.

Cytokine and chemokine analysis

We used the Luminex platform and a multiplex fluorescent bead array system (Bio-Rad) to quantify levels of nine factors (IL-1β, TNF-α, KC, MIP-2, MCP-1, IL-10, IL-12, GM-CSF, and IFN-γ) in BALF and whole-lung homogenates, using reagents purchased from R&D Systems. Commercially available ELISAs for MIP-1α and MIP-3α were purchased from R&D Systems and performed in a 96-well format per the manufacturer's

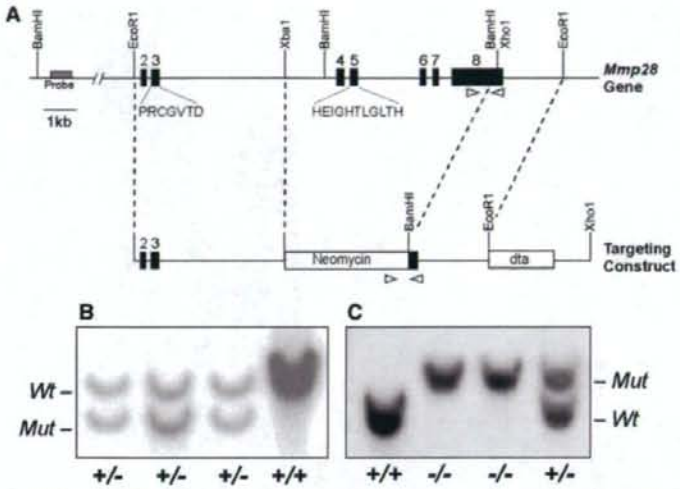

FIGURE 1. Generation of epilysin-null (*Mmp28*$^{-/-}$) mice. *A*, The targeting construct was designed to replace most of the exons, including exon 5, which codes for the catalytic domain. A diphtheria toxin cassette was included to select against ES cells with mistargeted recombination. The targeting construct was linearized with *Xho*I and injected in C57BL/6 blastocysts. After recombination, exons 4–7 and the full coding portion of the exon 8 are removed, and the epilysin transcript only contains exons 1–3 (coding for the proregion only). *B*, ES cell clones (144 total) were screened by Southern hybridization using a 694-bp probe in the 3′ terminal end of intron 1 just outside of the targeting construct. With *Bam*HI digestion, WT epilysin gene gives an ~9-kb band while targeted gene gives an ~7.5-kb band. *C*, F_1 offspring of chimeric mice were screened by Southern and PCR assays. For the PCR assay, the recombined locus produces a larger DNA fragment (324 nt) than that from the WT gene (259 nt) and both bands from heterozygotes. Three primers were used, the position and orientation of which are indicated by arrowheads: a WT forward primer, a neomycin cassette forward primer, and a common reverse primer.

protocol. Samples were performed in duplicate, and the data are normalized to a standard curve generated for each cytokine and expressed as pg/ml.

Immunostaining

Lung tissue from WT and *Mmp28*$^{-/-}$ mice were fixed in 10% formalin and paraffin-embedded. Sections were deparaffinized in HistoClear (National Diagnostics) and rehydrated through graded ethanol. Ag retrieval was performed using Ag unmasking solution (Vector Laboratories) heated to 90°C for 30 min. Endogenous peroxidase was blocked using 3% hydrogen peroxide for 10 min. Avidin and biotin block (Vector Laboratories) was applied to each section for 10 min. Sections were incubated with primary Ab for 1 h at 37°C and secondary Ab for 1 h at ambient temperature. After each incubation, the sections were washed three times in PBS. Secondary Abs were labeled with the Vectastain ABC kit, and colorimetric detection was done with diaminobenzidine staining per the manufacturer's protocol. Primary Abs were rat anti-mouse MAC-2 (gift of Dr. Elaine Raines, University of Washington) and rat anti-mouse neutrophil Ab (MCA771GA; AbD Serotec). Secondary Ab was donkey anti-rat HRP conjugated Ab (R&D Systems). Controls were processed with matching isotype control Ab.

Macrophage quantification was performed on tissue sections stained with MAC-2 and visualized at ×40 magnification. The number of stained cells was counted over a given area (160 mm^2) and averaged over 10 random fields.

Immunofluorescence

Lungs were inflated and embedded in Tissue-Tek OCT medium (Sakura Finetek), frozen in liquid nitrogen, and cut into 4- or 5-μm sections. Sections were incubated with goat serum (Jackson ImmunoResearch Laboratories) and avidin and biotin blocks. Sections were stained using a commercially available mouse-on-mouse immunodetection kit (Vector Laboratories) per the manufacturer's protocol. The primary Abs were mouse anti-human epilysin Ab (1/200; Cedarlane Laboratories), rabbit anti-CCSP Ab (1/10,000; gift of Barry Stripp, Duke University), and rat anti-mouse MAC-2 (1/300). Secondary Abs were biotin-conjugated anti-mouse Ab, Alexa Fluor 568 anti-rabbit Ab, and Alexa Fluor 568 anti-rat Ab. The biotin was identified using fluorescein-conjugated avidin. Costaining was performed using either epilysin and CCSP Abs or epilysin and MAC-2 Abs. Fluorescence was visualized using an Olympus BX51 microscope.

Leukocyte count and differential

For assessment of monocyte depletion 48 h after clodronate treatment, whole blood (0.7 ml/mouse) was obtained by cardiac puncture using a 25-gauge needle. The blood was diluted in an equal volume of PBS, layered on top of Histopaque 1077, and centrifuged per the manufacturer's protocol (Sigma-Aldrich). The monolayer of cells at the interface was removed, washed in PBS, and counted with a hemocytometer. Differentials were done on 30,000 cells cytospun onto slides and stained with LeukoStat (Fisher Scientific) (300 cells counted in random fields). Other cellular aliquots were incubated with anti-mouse CD16/CD32 mAb (BD Biosciences) at a concentration of 1 μg/10^6 cells for 10 min, and then anti-mouse CD11b-FITC mAb (BD Biosciences) at a concentration of 1 μg/10^6 cells for 60 min. After washing the cells in PBS plus 0.5% BSA, they were analyzed using a Beckman Coulter flow cytometer and CXP software.

Macrophages cultures

BMDM were derived from both WT and *Mmp28*$^{-/-}$ mice. Bone marrow from the femur and tibia was harvested under sterile technique. The marrow was recovered from the femur and tibia by brief centrifugation, and the pellet was resuspended in 500 μl of HBSS. Lysis of RBCs was performed using commercially available lysis buffer (eBioscience) per the manufacturer's protocol. After lysis, the cells were washed in PBS, resuspended in Mac medium (RPMI 1640 plus 10% FBS plus 20% supernatant from L929 cell line) and plated at a density of 1.5 × 10^6 cells/10-cm plate. Mac medium was changed on days 3 and 6. Between days 7 and 10, plates were washed twice using PBS to remove nonadherent or dead cells. The macrophages were then removed from the plate using a cell scraper, and cell counts and viability analysis were performed before chemotaxis studies.

Chemotaxis studies

Macrophage migration toward BALF was assessed with a fluorescence-based assay using 96-well chemotaxis chambers containing polycarbonate filters with 5-μm pores (ChemoTx; Neuro Probe). BMDM were incubated in RPMI 1640 containing 5 μg/ml calcein AM (Molecular Probes) and then washed and suspended at 4 × 10^6 cells/ml in phenol red-free RPMI 1640 (Sigma-Aldrich). Duplicate chamber wells were filled with BALF obtained from 8–10 WT or 8–10 *Mmp28*$^{-/-}$ mice exposed to aerosolized *P. aeruginosa*. Wells containing PBS were used to determine chemokinesis. The

chemotaxis membrane was applied and labeled macrophages (1×10^5 cells/25 μl) were placed directly onto the membrane. The chambers were incubated for 50 min at 37°C, nonmigrating cells on the top side of the membrane were removed, and fluorescence was determined in a fluorescence microtiter plate reader (CytoFluor II; PerSeptive Biosystems) in the bottom-read position. A standard curve from serial dilutions of macrophages was generated to determine the number of cells migrating to the bottom well. Chemokinesis, or random migration, with PBS in the bottom well was calculated and subtracted from all values when calculating percentage migration. In a separate experiment, WT and *Mmp28*$^{-/-}$ BMDM were stimulated with 100 ng of *Escherichia coli* LPS strain O111:B4 (Sigma-Aldrich) or medium alone 24 h before harvest. Triplicate chamber wells were filled with BALF obtained from a WT mouse instilled with *P. aeruginosa* 24 h before harvest. LPS-stimulated and medium-alone WT and *Mmp28*$^{-/-}$ BMDM were placed on top of the membrane as described above and assessed for chemotaxis after 50 min of incubation at 37°C.

BMDM activation

BMDM were isolated and cultured as described above. Macrophages were transferred to 12-well plates at a density of 1×10^6 cells/well. The cells were stimulated with 100 ng of *E. coli* LPS strain O111:B4 or infected with 5×10^6 CFU of *P. aeruginosa* PAK strain in DMEM culture medium for 2 h at 37°C, 5% CO_2. After 2 h, cells were washed twice with PBS containing 0.1% gentamicin (Invitrogen) and incubated with DMEM, 0.1% gentamicin. Cells were collected at 24, 48, or 72 h for qRT-PCR. Unstimulated macrophages served as a control.

Data analysis

Results are expressed as means ± SEM. Statistical significance was determined using Student's *t* test. Differences were considered significant if the *p* value was <0.05.

Results

Epilysin-null mice

The targeting construct was designed to delete exons 4–8, which include the catalytic domain (Fig. 1*A*). The construct contained expression cassettes for neomycin resistance (positive selection) and diphtheria toxin sensitivity (negative selection). After homologous recombination, exons 4–7 and the full coding portion of the exon 8 were excised, and any transcript produced would contain only exons 1–3 (coding for the proregion only). We screened 144 neomycin-resistant ES cell clones, and of these, 4 indicated homologous recombination (Fig. 1*B*). Chimeric mice were bred to C57BL/6 mice to generate germline heterozygotes. These mice were then backcrossed to yield homozygous null (*Mmp28*$^{-/-}$) mice (Fig. 1*C*). These mice have been backcrossed to C57BL/6NTac mice for 10 generations. Homozygous *Mmp28*$^{-/-}$ mice are healthy with no defects in fertility, litter size, weight gain (at least up to 6 mo), behavior, or tissue morphology. Additionally, their airways appear normal with the expected proportion of ciliated and Clara cells. As verified by RT-PCR, no epilysin mRNA is detected in these mice (data not shown).

Epilysin is expressed by Clara cells and macrophages

In mice, epilysin is expressed in a number of adult tissues, with the highest levels seen in lung (18). By immunofluorescence, epilysin localized to the airway epithelium (Fig. 2*A*) and colocalized with CCSP (Fig. 2*B*), indicating that this MMP is produced by Clara cells. To confirm these findings, lung tissue from *Mmp28*$^{-/-}$ mice did not demonstrate staining in the airway epithelia (Fig. 2*A*). Furthermore, we collected an enriched population of Clara cells using LCM of cells at the bronchoalveolar junction (which is comprised of ~90% Clara cells). qRT-PCR for CCSP verified an enrichment of Clara cells (data not shown), and qRT-PCR for MMP-28 confirmed that Clara cells express epilysin mRNA (Fig. 2*C*). In contrast, matrilysin (MMP-7) is seen only in ciliated and basal cells and not in Clara cells (25–27), indicating that these two epithelial MMPs serve nonoverlapping functions in lung biology.

Analysis of mRNA by qRT-PCR collected from freshly isolated alveolar macrophages revealed no expression of epilysin (*Ct* value of 35.1 ± 0.23). Additionally, no immunofluorescence signal was seen in alveolar macrophages stained with an epilysin Ab (data not shown). However, resting BMDM did express epilysin, albeit at relatively low levels (*Ct* value of 31.59 ± 1.18). These findings suggest that epilysin is expressed by a subset of macrophages, and that localization or differentiation within the tissue may change epilysin expression patterns.

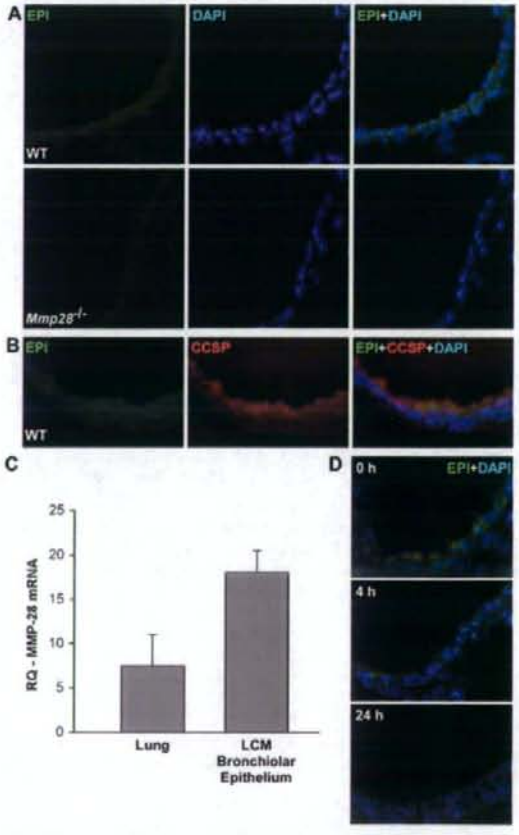

FIGURE 2. MMP-28 is expressed by Clara cells in the lung. *A*, Immunofluorescence staining for epilysin in the airway epithelium from naive WT mice (*top panel*) compared with *Mmp28*$^{-/-}$ mice (*bottom panel*). Nuclei were labeled with 4′,6-diamidino-2-phenylindole (DAPI), demonstrating epilysin expression in the cytoplasm of airway epithelial cells. *B*, Co-immunostaining of epilysin and CCSP (Clara cell marker). *C*, MMP-28 mRNA from whole-lung and LCM-retrieved bronchiolar epithelium. MMP-28 expression is enriched in LCM-retrieved bronchiolar epithelium compared with whole lung. Samples were normalized to β_2-microglobulin. *D*, Immunofluorescence staining for epilysin in the airway epithelium from naive WT mice (0 h), and *P. aeruginosa*-treated mice harvested at 4 and 24 h after infection. Immunostaining demonstrates decreased epilysin levels in the airway epithelium from infected mice.

Disparate control of epilysin expression by epithelial cells and macrophages in response to infection

We examined the temporal expression of epilysin and other MMPs in response to *P. aeruginosa* infection by qRT-PCR. Lungs from four to five mice per genotype were collected and processed for RNA at 0, 4, 24, 48, and 96 h after pulmonary infection with

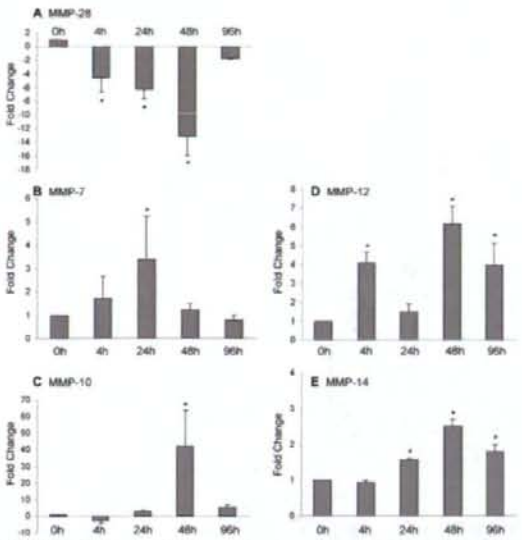

FIGURE 3. Lung MMP expression in response to *P. aeruginosa* pneumonia. Whole-lung RNA was collected at serial times after exposure to *P. aeruginosa* and levels of specific transcripts were determined by qRT-PCR and normalized to HPRT. Reported are fold change in mRNA levels relative to time 0. *A*, MMP-28 expression was rapidly down-regulated and returned to baseline after resolution of infection and inflammation. *B–E*, In contrast to MMP-28, other MMPs (MMP-7, -10, -12, and -14) were induced during infection. *, $p < 0.05$ compared with time point 0; $n = 4–5$ mice/time point.

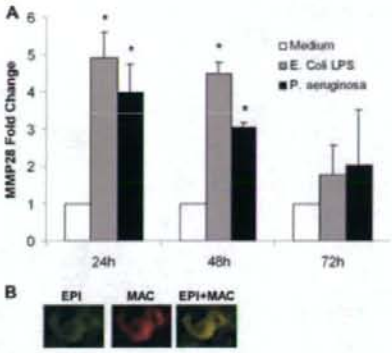

FIGURE 4. Up-regulation of MMP-28 expression in macrophages. *A*, BMDM were incubated in medium alone, *E. coli* LPS, or *P. aeruginosa*, and mRNA was collected for qRT-PCR analysis at 24, 48, and 72 h post-exposure. MMP-28 expression by BMDM was stimulated by both LPS and *P. aeruginosa* at 24 and 48 h. Samples were normalized to HPRT. *, $p < 0.05$ when compared with time-controlled medium alone samples. *B*, Immunofluorescence staining for epilysin and MAC-2 48 h after *P. aeruginosa* exposure in WT mice. Images demonstrate coexpression of epilysin and MAC-2 in selected macrophages.

P. aeruginosa. Unlike matrilysin (MMP-7), stromelysin-2 (MMP-10), macrophage metalloelastase (MMP-12), and membrane type-1 MMP (MMP-14), which are all up-regulated or induced in response to airway infection (27, 28), epilysin was rapidly down-regulated >4-fold within 4 h postinfection (Fig. 3). Although its mRNA levels dropped markedly, the *Ct* values at 24 h (25.69 ± 0.48) indicated that expression of epilysin was still maintained at relatively high levels. By 96 h postinfection, by which time the bacteria were cleared (see Fig. 7) and the neutrophilic inflammation had resolved (data not shown), the expression of epilysin rebounded, approaching preinfection levels (Fig. 3*A*). Similarly, in response to *P. aeruginosa*, we saw reduced signal for epilysin protein by immunofluorescence. Both the number of positive airway cells and intensity of staining decreased during infection (Fig. 2*D*). We did not observe differences in mRNA expression of MMP-7, -10, or -14 mRNAs in either naive or infected lungs of *Mmp28*$^{-/-}$ and WT mice (data not shown).

In contrast, the expression pattern of epilysin by BMDM differed from that of epithelial cells. Both bacteria (*P. aeruginosa*) or LPS (from *E. coli*) up-regulated epilysin expression by BMDM (Fig. 4*A*). We did not detect epilysin expression in resident macrophages in the lung by immunohistochemistry (data not shown), but by 48 h after infection with *P. aeruginosa*, 33.3 ± 5.2% of pulmonary macrophage express epilysin based on coimmunofluorescence with MAC-2 and epilysin Abs (Fig. 4*B*). Collectively, these data indicate disparate regulation of epilysin by epithelium and leukocytes and suggest different roles of epilysin in epithelial and leukocyte biology. Furthermore, the decrease in epilysin mRNA expression in the injured lung likely reflects the contribution of epithelial-derived epilysin. Although epilysin is expressed in cultured BMDM, the fact that it is not detected in resident macrophages in naive lung suggests that multiple factors may interact to regulate its expression, and bacterial stimulation is one factor.

Altered macrophage recruitment in Mmp28$^{-/-}$ *mice*

Because many MMPs function in immunity (6), we assessed whether epilysin has immunoregulatory functions. To test this idea, we compared the inflammatory response between WT and *Mmp28*$^{-/-}$ mice challenged with *P. aeruginosa*. Mice were exposed to aerosolized *P. aeruginosa* to achieve a deposition of ~5 × 10^5 bacteria/lung. The lungs were harvested at 4 and 24 h postinfection for BALF cell counts, differential, histology, bacterial counts, and cytokine analysis. At 4 h postinfection, we detected no significant difference in the total number of cells in BALF from *Mmp28*$^{-/-}$ and WT mice (Fig. 5*A*). While 79–94% of the total cells where neutrophils at this time, their numbers did not differ significantly between genotypes (Fig. 5*B*). However, at 4 h postinfection, *Mmp28*$^{-/-}$ mice had a markedly enhanced (6-fold) increase in BALF macrophages compared with infected WT mice (Fig. 5, *C* and *D*). Importantly, uninfected WT and *Mmp28*$^{-/-}$ mice did not differ in their macrophage numbers in BALF or whole-lung extracts, and they also had similar numbers of circulating monocytes (data not shown). These data indicate that the increased number of macrophages recovered from the lungs of infected *Mmp28*$^{-/-}$ mice reflected an accelerated influx and not an increased population of resident macrophages.

By 24 h postaerosolization, the increase in total BALF cells observed in WT mice was significantly blunted in *Mmp28*$^{-/-}$ mice (7.14 ± 0.82 × 10^6 vs 4.97 ± 0.54 × 10^6 cells in WT vs *Mmp28*$^{-/-}$ mice, respectively), which was due to a lesser increase in neutrophils (Fig. 5, *A* and *B*). At this time, we no longer saw a difference in the recovery of BALF macrophage between genotypes.

Evaluation of the lung histology by immunohistochemistry for a macrophage-specific marker, MAC-2 (29), demonstrated increased influx of macrophages in *Mmp28*$^{-/-}$ compared with WT mice (16.4 ± 4.2 vs 7.2 ± 2.4 cells/160 mm^2, $p < 0.05$) (Fig. 6). In our evaluation of lung sections, labeled with a neutrophil-specific marker, we saw no evidence that neutrophils in *Mmp28*$^{-/-}$ mice

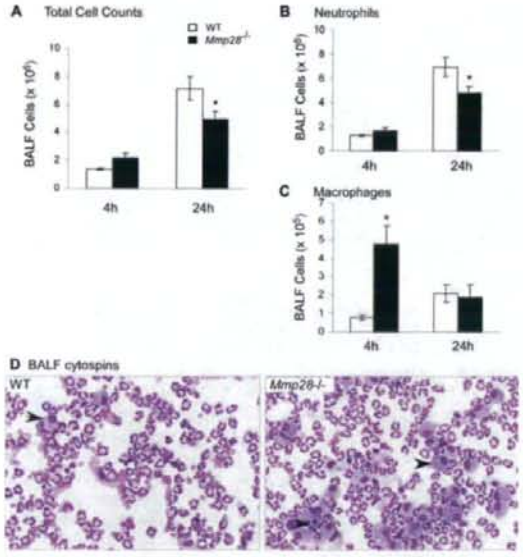

FIGURE 5. BALF cell counts following *P. aeruginosa* challenge. WT (open bars) and *Mmp28*$^{-/-}$ mice (filled bars) mice were exposed to aerosolized *P. aeruginosa* and harvested at 4 and 24 h for BALF cell counts and differential. *A*, Total cell counts, demonstrating significantly reduced cell counts at 24 h in *Mmp28*$^{-/-}$ mice. *B*, Total neutrophils (PMNs), demonstrating reduced neutrophil recruitment at 24 h in the *Mmp28*$^{-/-}$ mice, and (*C*) total macrophages (MACs), demonstrating increased early macrophage recruitment at 4 h in *Mmp28*$^{-/-}$ mice. *, $p < 0.05$. *D*, Representative cytospins of BALF collected 4 h after *P. aeruginosa* infection in WT and *Mmp28*$^{-/-}$ mice. Arrowheads point to macrophages. Data are means ± SEM; results represent 10 mice/time point.

were sequestered elsewhere in the lung (Fig. 6). Thus, the slightly reduced neutrophils numbers observed in the lavage of *Mmp28*$^{-/-}$ mice at 24 h postinfection (Fig. 5*B*) cannot be attributed to impaired migration through lung tissue, as seen in other MMP-deficient mice (Fig. 6) (9).

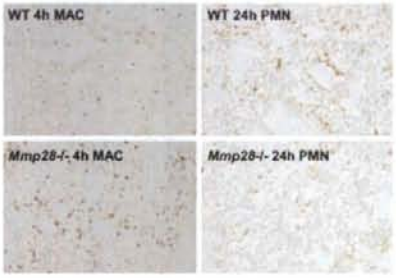

FIGURE 6. Lung histology after *P. aeruginosa* inhalation. These are representative images demonstrating enhanced macrophage influx into the lung of *Mmp28*$^{-/-}$ mice at 4 h postinfection with *P. aeruginosa* (*bottom left*), and reduced neutrophil influx into the lung of *Mmp28*$^{-/-}$ mice 24 h postinfection with *P. aeruginosa* (*bottom right*) compared with WT controls (*top*). Lungs were fixed in 10% formalin, paraffin-embedded, and stained with anti-mouse MAC-2 Ab (*left*) or anti-neutrophil Ab (*right*). Secondary Ab was HRP-conjugated donkey anti-rat Ab. Secondary Abs were labeled with the Vectastain ABC kit, and colorimetric detection was done with diaminobenzidine staining.

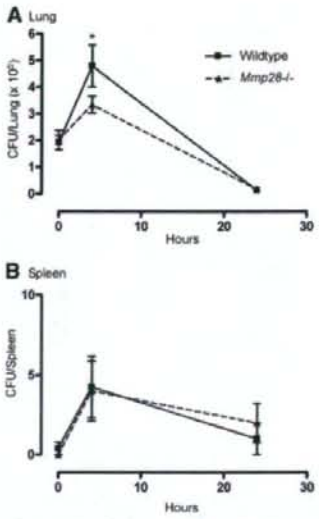

FIGURE 7. *P. aeruginosa* clearance from the lung at 4 and 24 h following bacterial challenge in WT and *Mmp28*$^{-/-}$ mice. Mice were exposed to aerosolized *P. aeruginosa*, and lungs and spleens (a surrogate marker for bacteremia) were harvested at 0, 4, and 24 h for bacterial counts. Results are expressed as CFU per lung or spleen. *A*, At 4 h, CFU in the lung are significantly decreased in *Mmp28*$^{-/-}$ mice vs WT control. +, $p < 0.05$. *B*, There is no difference in CFU from the spleen between genotypes. Data are means ± SEM; results are from $n = 10$ mice/time point.

Enhanced P. aeruginosa *clearance in* Mmp28$^{-/-}$ *mice*

Infected *Mmp28*$^{-/-}$ mice had enhanced *P. aeruginosa* clearance from their lungs at 4 h (Fig. 7*A*). However, by 24 h postinfection, both WT and *Mmp28*$^{-/-}$ mice had efficiently cleared the bacteria. There was no significant bacteremia between genotypes as measured by the recovery of live bacteria from homogenates of spleen (Fig. 7*B*).

Macrophages are required for P. aeruginosa *clearance*

Our data suggest that macrophages contribute to clearance of *P. aeruginosa* from the lung and, possibly as a result of this, neutrophil recruitment. To assess if accelerated macrophage recruitment in *Mmp28*$^{-/-}$ mice led to faster bacterial clearance and reduced neutrophil influx to the lungs of infected *Mmp28*$^{-/-}$ mice, we depleted alveolar and circulating monocytes from WT and *Mmp28*$^{-/-}$ mice by intranasal and i.p. administration of clodronate coupled with liposomes. Control mice received the liposome carrier by both routes. Clodronate is a common agent used to deplete selected populations of macrophages and monocytes in vivo and, when coupled with liposomes, it allows for the intracellular introduction and accumulation of clodronate in macrophages, resulting in apoptosis (30–32).

Forty-eight hours after clodronate treatment, mice were harvested to determine the efficacy of macrophage depletion in both the lung and circulation. We observed a 10-fold reduction in alveolar macrophage numbers (Fig. 8*A*) and a partial reduction in circulating monocytes, particularly a reduction in CD11b^{high} monocytes (Fig. 8, *B* and *C*). Neutrophil influx into the lungs did not differ significantly between both clodronate and liposome-only groups (Fig. 8*A*), and the lung histology demonstrated no evidence of lung injury (data not shown). Immunostaining with MAC-2 Ab confirmed a reduction of pulmonary macrophages (Fig. 8*A*).

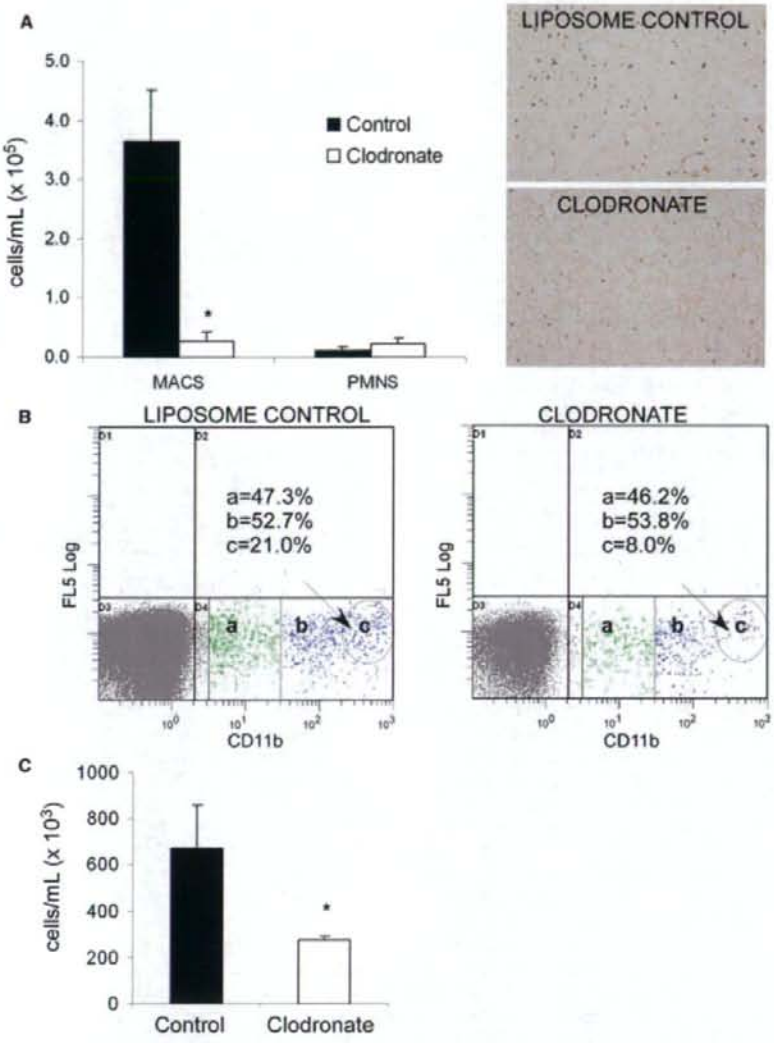

FIGURE 8. Macrophage depletion using clodronate. Alveolar macrophages and circulating monocytes were depleted using intranasal and i.p. clodronate, respectively. Control mice received intranasal and i.p. liposome only. Forty-eight hours after treatment, mice were harvested for BALF, lung histology, and circulating leukocyte cell counts and differential. Lungs were inflated with 10% formalin and embedded in paraffin. Sections were stained with MAC-2 to analyze pulmonary macrophage content. *A*, BALF cell count and differential demonstrating a 10-fold reduction in alveolar macrophages with no significant difference in neutrophil recruitment in clodronate-treated mice. Immunostaining confirmed a significant reduction of pulmonary macrophages in the clodronate-treated group. *B*, Flow cytometry of circulating leukocytes. Leukocytes were isolated from liposome-treated (*left*) and clodronate-treated (*right*) mice using gradient separation with Histopaque 1077. Cells were stained with FITC-conjugated anti-mouse CD11b and analyzed by flow cytometry. The dot plots represent the $CD11b^+$ population of leukocytes, with CD11b staining intensity on the *x*-axis. The $CD11b^+$ cells are grouped into three subgroups (*a*–*c*) based on level of expression. The percentages represent numbers of $CD11b^+$ cells in area/total $CD11b^+$ cells. Clodronate-treated mice demonstrated depletion of a $CD11b^{high}$ population of circulating monocytes (*c*) from 21% to 8% of all $CD11b^+$ cells (*a*–*c*). *C*, Total circulating monocyte cell counts as determined by manual differential and cell counts from control and clodronate-treated WT mice. There was a significant reduction in the numbers of circulating monocytes in clodronate-treated mice. *, $p < 0.05$.

We instilled *P. aeruginosa* into the lungs of macrophage-depleted (clodronate) WT and *Mmp28*$^{-/-}$ mice and liposome-only (control) WT and *Mmp28*$^{-/-}$ mice. Compared with control WT mice, macrophage-depleted WT mice had increased neutrophil influx into BALF at 4 and 24 h (Fig. 9*A*), yet impaired bacterial clearance at 4 h (Fig. 9*C*). Increased neutrophils and impaired bacterial clearance were also observed in *Mmp28*$^{-/-}$ mice treated with clodronate (Fig. 9, *A* and *C*). Furthermore, bacterial clearance at 4 h and neutrophil recruitment at 24 h did not differ between WT and *Mmp28*$^{-/-}$ macrophage-depleted mice (Fig. 9, *A* and *C*). These results indicate that macrophages aid in the clearance of *P. aeruginosa* from the lung and modify the inflammatory response to these bacteria, and they provide further evidence that accelerated macrophage recruitment in *Mmp28*$^{-/-}$ mice (Figs. 5*C* and 9*B*) contributes to faster bacterial clearance and reduced neutrophil recruitment.

Altered chemokines and cytokines in Mmp28$^{-/-}$ *mice*

Given the above differences in macrophage and neutrophil recruitment, we assessed if levels of neutrophil and macrophage chemokines and other cytokines in BALF and whole-lung homogenates differed between *P. aeruginosa*-infected WT and *Mmp28*$^{-/-}$ mice. For this, we used a multiplex cytokine/chemokine assay on a Luminex platform. Nine cytokines (IL-1β, TNF-α, KC, MIP-2, MCP-2, IL-10, IL-12, GM-CSF, and IFN-γ) were assessed from BALF and lung homogenates from WT and *Mmp28*$^{-/-}$ mice at 4 and 24 h postinfection. The levels of two additional macrophage chemokines, MIP-1α and MIP-3α, in BALF and lung homogenates were assessed by ELISA.

Consistent with reduced neutrophilia in *Mmp28*$^{-/-}$ mice (Fig. 5*B*), we found slightly reduced levels of the CXC chemokines KC and MIP-2 in both BALF and lung homogenates from *Mmp28*$^{-/-}$ mice at 4 h postinfection (Fig. 10). Because KC and MIP-2 levels

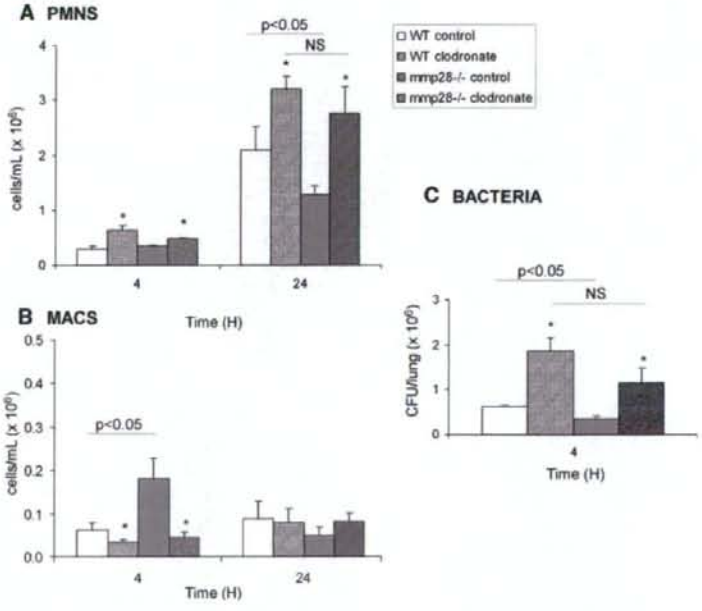

FIGURE 9. Macrophage-deficient mice have impaired bacterial clearance and increased pulmonary neutrophilia. Results from control WT (open bar) and *Mmp28*$^{-/-}$ (gray bar) mice vs clodronate-treated WT (white striped bar) and *Mmp28*$^{-/-}$ (gray striped bar) mice. All groups have been treated with intranasal instillation of *P. aeruginosa* (1×10^7 organisms/lung) and harvested at 4 and 24 h for BALF cell counts, differential, and bacterial clearance. *A*, BALF neutrophil cell counts at 4 and 24 h postinfection. *B*, BALF macrophage cell counts at 4 and 24 h postinfection. *C*, Whole-lung bacterial counts (CFU) 4 h after infection. *, $p < 0.05$ when compared with same genotype mice.

were reduced in both the alveolar (BALF) and tissue compartments, it is likely that the lack of epilysin affected chemokine expression and not the formation of chemokine gradients. Importantly, we found that the levels of MCP-1, a potent macrophage chemokine, in the BALF or tissue homogenates did not differ between infected WT and *Mmp28*$^{-/-}$ mice. There was no difference in MIP-1α levels, and there was a slight decrease in MIP-3α at 4 h in the *Mmp28*$^{-/-}$ BALF compared with WT. Thus, the rapid and early influx of macrophages seen in the *Mmp28*$^{-/-}$ mice was apparently not mediated by an increase in chemokine expression or altered chemokine gradient.

We also found that TNF-α, IL-6, and GM-CSF were increased in *Mmp28*$^{-/-}$ BALF at 4 h, but not 24 h. Because these cytokines are produced by macrophages, the increased levels at 4 h may reflect the increased number of pulmonary macrophages in the *Mmp28*$^{-/-}$ mice. We did not detect any significant differences in IL-1β, IL-10, IL-12, or IFN-γ (not shown).

Enhanced chemotaxis of Mmp28$^{-/-}$ *BMDM*

The chemokine data suggested that the more rapid influx of macrophages into *Mmp28*$^{-/-}$ was not due to altered levels of chemotactic activity. We then assessed if the accelerated macrophage recruitment seen in vivo was due to enhanced migratory ability of *Mmp28*$^{-/-}$ macrophage. For this, we compared the chemotaxis of BMDM from WT and *Mmp28*$^{-/-}$ mice to move toward unconcentrated, cell-free BALF obtained from 8–10 *P. aeruginosa*-infected WT or 8–10 *Mmp28*$^{-/-}$ mice (PA BALF).

Although the chemoattractant activity in PA BALF was modest, we observed a small decrease in the chemoattractant activity in PA BALF from *Mmp28*$^{-/-}$ compared with WT mice (Fig. 11*A*). This diminished activity in the *Mmp28*$^{-/-}$ PA BALF may be due to greater clearance of chemokines and other bacterial factors by the augmented macrophage numbers. In agreement with the chemokine data, these findings indicate that epilysin does not restrain macrophage influx by affecting the activity of chemotactic factors.

Interestingly, we observed an enhanced ability of the *Mmp28*$^{-/-}$ BMDM to migrate to PA BALF of either genotype (Fig. 11), and no difference in chemokinesis or random migration to PBS (not shown). Although *P. aeruginosa* or *E. coli* LPS stimulated epilysin expression by BMDM (Fig. 5), up-regulation of this proteinase did not further affect BMDM migration (Fig. 11*B*). These data suggest that the basal level of epilysin expression is sufficient to govern the migratory ability of BMDM. Furthermore, because BMDM express epilysin and because they would not be exposed to epithelial-derived epilysin in this culture model, these data also indicate that epilysin retards macrophage influx by a cell-autonomous mechanism.

Discussion

The broad expression of epilysin in naive tissue and the rapid down-regulation of total levels in response to infection, unlike that of many other MMPs, suggest that this proteinase serves a unique role among its family members. Although the constitutive expression of epilysin in many tissues suggest that this proteinase functions in homeostasis, *Mmp28*$^{-/-}$ mice, similar to other MMP-deficient mice, have no overt phenotype in the unchallenged state. We have found, however, increased deposition of elastin in the lungs of *Mmp28*$^{-/-}$ mice compared with WT animals (our unpublished observations), suggesting that the basal expression of epilysin may function in the epithelial control of interstitial matrix production. Regardless of this phenotype, the null mice are overtly normal.

Although the lack of phenotype in unchallenged *Mmp28*$^{-/-}$ mice might imply compensation by another MMP, we have found neither altered nor aberrant expression of other epithelial MMPs. An alternative possibility is that epilysin functions in innate immunity and, hence, a phenotype would not be revealed until this system is challenged. Indeed, when we infected *Mmp28*$^{-/-}$ mice with *P. aeruginosa*, we observed accelerated macrophage recruitment into their lungs by 4 h, compared with the infiltration seen in

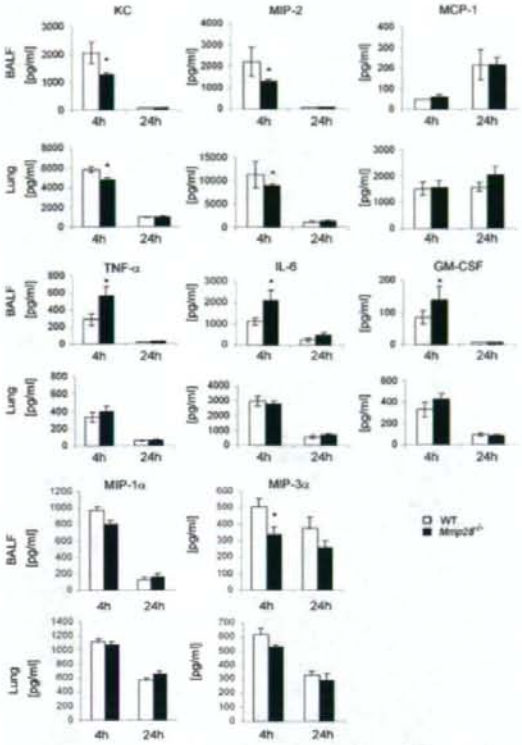

FIGURE 10. BALF and lung homogenate cytokines. WT (open bars) and *Mmp28*$^{-/-}$ mice (filled bars) were exposed to aerosolized *P. aeruginosa* and harvested at 4 and 24 h for whole-lung homogenates of the right lung, and BALF from the left lung. The levels of several chemokines and cytokines were assessed from these two compartments using Luminex-based assays and ELISAs. KC and MIP-2 are significantly decreased in the BALF and whole-lung homogenates of *Mmp28*$^{-/-}$ mice 4 h postinfection. There is no difference in MCP-1 or MIP-1α levels. TNF-α, IL-6, and GM-CSF are significantly increased in the BALF, but not whole-lung homogenates, of *Mmp28*$^{-/-}$ mice 4 h postinfection. Data are means ± SEM; results represent 10 mice/time point. *, $p < 0.05$.

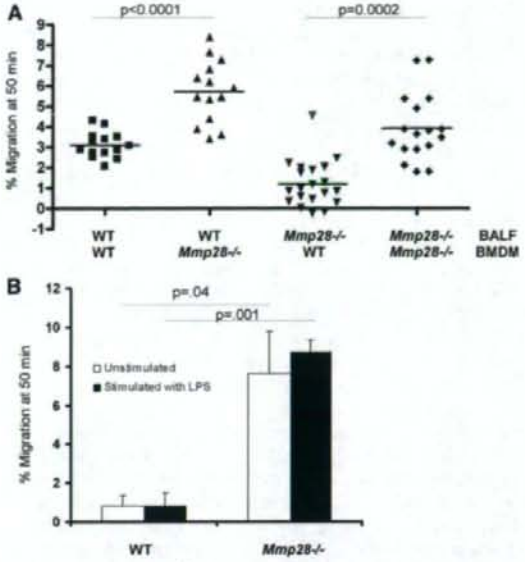

FIGURE 11. *Mmp28*$^{-/-}$ macrophages migrate faster than do WT cells. *A*, Migration of WT and *Mmp28*$^{-/-}$ BMDM to BALF obtained from *P. aeruginosa*-treated WT or *Mmp28*$^{-/-}$ mice. At 50 min, *Mmp28*$^{-/-}$ BMDM migrated faster to all BALF samples compared with WT BMDM. There was a slight decrease in chemoattractant activity in BALF from *Mmp28*$^{-/-}$ compared with WT mice. *B*, *Mmp28*$^{-/-}$ vs WT BMDM migrated faster to WT BALF. LPS-stimulated BMDM (filled bars) did not affect chemotaxis of BMDM compared with unstimulated cells (open bars).

WT mice. At 24 h postinfection, we saw no difference in macrophage recruitment between genotypes, likely reflecting redundant mechanisms involved in their later recruitment. Furthermore, bacterial clearance was accelerated and neutrophil recruitment was blunted in *Mmp28*$^{-/-}$ mice, which we predict are consequences of accelerated macrophage recruitment. Supporting this idea, we found that macrophage depletion in WT and *Mmp28*$^{-/-}$ mice resulted in impaired 4 h clearance of *P. aeruginosa* with increased 4 and 24 h neutrophil recruitment to the lung. Overall, our results suggest that epilysin serves as a negative regulator of macrophage recruitment by inhibiting the chemotaxis of macrophages.

In naive lung, epilysin is expressed by airway Clara cells and is not expressed by resident pulmonary macrophages. Epilysin is also constitutively expressed by BMDM. In response to infection, expression of epilysin by epithelial cells is rapidly down-regulated, but it is up-regulated in pulmonary macrophages and BMDM. These findings indicate disparate regulation of epilysin by epithelium and leukocytes and suggest different roles of epilysin in epithelial and leukocyte biology. Furthermore, our findings indicate that the endogenous expression of epilysin by macrophages is sufficient to retard their early recruitment into the lung. Indeed, in both in vivo and cell-based models, epilysin-dependent effects on macrophage influx and chemotaxis were evident at early times: 4 h in vivo and <1 h in isolated cells.

Of the many MMPs that function in immunity, most do so by cleaving specific proteins, often resulting in a gain-of-function activity for the target substrate (5). Authentic and potential MMP substrates that regulate inflammatory responses include antimicrobial peptides, cytokines, chemokines, chemokine receptors, and accessory proteins that bind, retain, or concentrate chemokines (6). For example, IL-1β can be activated by several MMPs (MMP-2, -3, and -9) (33) and MMP-7 and MMP-12 have been reported to activate latent TNF-α in isolated macrophages (12, 34, 35). In addition to cytokines, several MMPs process chemokines making them more or less potent (14, 36–38) or by generating chemoattractant peptides from precursor proteins (39). For example, the N-terminal domain of CXCL8 (IL-8) and LIX (the mouse equivalent of CXCL5 and CXCL6) are processed by MMP-9 and MMP-8, respectively, resulting in products that have more potent chemoattractant activities than do the full-length molecules (14, 36). MMPs can also affect chemokine gradients by shedding accessory proteins that bind or restrain chemokines. Work in our laboratory demonstrated that matrilysin promotes neutrophil efflux into the alveolar space via shedding of transmembrane proteoglycan syndecan-1 complexed with KC, a murine CXC chemokine (9).

MCP-1 is the predominant macrophage chemokine regulating monocyte recruitment to the lung via its interaction with its receptor, CCR2 (40). Based on our observations of accelerated macrophage recruitment in infected *Mmp28*$^{-/-}$ mice, we examined the lung and bronchoalveolar compartments for altered MCP-1 levels or gradients. At both 4 and 24 h, we found similar levels of MCP-1

in the BALF and whole-lung homogenate between the *Mmp28*$^{-/-}$ and WT mice. A similar finding was observed for other macrophage chemokines, MIP1-α and MIP3-α. Thus, the rapid and early influx of macrophages seen in the *Mmp28*$^{-/-}$ mice was apparently not mediated by chemokine production or gradient formation.

Since some MMPs can cleave chemokines, making them more or less potent, we also examined the chemoattractant activity of BALF recovered from *P. aeruginosa*-treated WT and *Mmp28*$^{-/-}$ mice (6). Using macrophages cultured from bone marrow from WT and *Mmp28*$^{-/-}$ mice in a chemotaxis assay, we did not observe an increase in the chemoattractant activity from BALF recovered from the *Mmp28*$^{-/-}$ mice. In fact, we observed a slight decrease in the chemoattractant activity in the BALF from *Mmp28*$^{-/-}$ compared with WT mice. The diminished activity in the *Mmp28*$^{-/-}$ BALF may be due to greater clearance of chemokines by the augmented macrophage numbers. Based on these findings, it is unlikely that epilysin affected macrophage recruitment via enhanced chemokine gradients. Using this same chemotaxis assay, we observed an enhanced ability of the *Mmp28*$^{-/-}$ macrophages to migrate to BALF of either genotype. These data indicate that epilysin expression by macrophages retards the ability of macrophages to migrate to chemoattractants. Interestingly, we found that *P. aeruginosa* or *E. coli* LPS stimulated epilysin expression by BMDM. However, this up-regulation did not further affect BMDM migration, suggesting that the basal levels of this MMP are sufficient to restrain BMDM response to chemoattractants. Thus, epilysin may have additional unidentified roles in macrophage biology. Epilysin alters early migration, but later recruitment is likely mediated by redundant or more potent mechanisms.

The chemokine receptor for MCP-1, CCR2, is a critical determinant of monocyte recruitment, and studies of CCR2-deficient mice demonstrate significantly reduced monocyte/macrophage influx in models of peritonitis or lung injury (40, 41). Although we found no evidence of an altered MCP-1 gradient, proteolysis of CCR2 on infiltrating macrophages could slow their advancement at the early stages of inflammation. We examined the expression of CCR2 on macrophages isolated from the peritoneum of naive WT and *Mmp28*$^{-/-}$ mice and observed no difference in baseline CCR2 levels (not shown). Additionally, we evaluated the expression of CCR2 on our unstimulated BMDM and observed all of our macrophages express this chemokine receptor with no difference in expression between our WT and *Mmp28*$^{-/-}$ mice (not shown). These data suggest that epilysin does not alter CCR2 expression or CCR2 shedding. Macrophages can express additional chemokine receptors, such as CCR1, CCR5, CCR6, and CXCR3; however, these chemokine receptors appear less important in chemotaxis, as only a small subset of macrophages expresses these receptors (42, 43). Careful analysis of macrophage chemotaxis to various recombinant chemokines may prove useful in further identifying a chemokine receptor that may be an MMP-28 substrate.

Alternatively, epilysin may regulate macrophage influx by shedding an adhesive protein. To migrate across vascular endothelium in vitro, human monocytes utilize sequential interactions of members of the selectin family (L-selectin), α_4 integrins (VLA-4 and VLA-5), α_2 integrins (CD11c/CD18), and PECAM-1 with endothelial selectins ICAM-1, VCAM-1, and PECAM-1 (44–47). Adhesive interactions on the epithelial side include VLA-4, VLA-5, VLA-6, CD11a, CD11b, CD11c/CD1,8 and CD47 on human monocytes (44). In mice, however, monocyte recruitment into lung is dependent on monocyte expression of CD11a, CD11b, ICAM-1, and VLA-4 (48). Recently, the neural cell adhesion molecule NCAM has been shown to be an in vitro substrate for *Xenopus* MMP-28 (49), and other Ig domain cell adhesion proteins may also be potential substrates. Other mechanisms, such as delayed apoptosis, could also contribute to increased macrophage numbers in the *Mmp28*$^{-/-}$ mice; however, they are likely not involved given these early time points.

In addition to our findings related to epilysin-mediated macrophage recruitment, our study demonstrates a key protective role for macrophages in *P. aeruginosa* pneumonia. To date, only two studies have examined the role of the alveolar macrophage in *P. aeruginosa* pneumonia, each with opposing findings. Cheung et al. found no difference in *P. aeruginosa* clearance from the lung in macrophage-depleted vs control mice (50). However, Kooguchi et al., who achieved greater macrophage depletion than Cheung et al., found that macrophage-depleted mice had delayed clearance of *P. aeruginosa*, delayed but sustained neutrophil recruitment to the alveolar spaces, and increased lung injury and mortality compared with control mice (30). Our findings are consistent with those of Kooguchi et al. and indicate that macrophages contribute modestly to *P. aeruginosa* clearance, and reduction of the macrophage population leads to significantly more pulmonary neutrophilia. Although the change in neutrophil influx may be due to other effects mediated by macrophages, delayed bacterial clearance is a likely contributor. In a different model of *P. aeruginosa* infection in the cornea of macrophage-depleted mice, a similar finding of impaired *P. aeruginosa* clearance and increased neutrophil recruitment was observed (51). This relationship of the macrophage to neutrophil recruitment is also consistent with our findings of reduced 24 h neutrophil recruitment to the lung in the *Mmp28*$^{-/-}$ mice. Since loss of neutrophil recruitment in *Mmp28*$^{-/-}$ mice may be due to altered chemokine gradients, we examined the levels of KC and MIP-2 chemokines in both whole lung and BALF. These neutrophil chemokines were reduced in both compartments (whole lung and BALF), suggesting that epilysin affected KC and MIP-2 expression but not gradient formation. We also examined the lungs of *Mmp28*$^{-/-}$ mice using immunostaining for neutrophils, and there was no evidence that neutrophils were sequestered elsewhere in the lung. Thus, the reduced neutrophil numbers seen in the BALF of *Mmp28*$^{-/-}$ mice at 24 h postinfection cannot be attributed to impaired migration through lung tissue. Our findings indicate that the lower BALF neutrophil levels in *Mmp28*$^{-/-}$ mice are due to blunted chemokine signals, likely a consequence of reduced bacterial replication in *Mmp28*$^{-/-}$ mice.

Overall, our results indicate that epilysin serves as a negative regulator of early macrophage recruitment, and this novel function may have evolved as a mechanism to restrain unnecessary and untimely inflammation. Future studies will be aimed at substrate identification to determine how epilysin restrains macrophage influx.

Acknowledgments

We thank Ronald McCarthy and Dale Kobayashi (Washington University) for helping generate knock-out mice, Elaine Raines (University of Washington) for kindly providing the MAC-2 Ab, Barry Stripp (Duke University) for providing the anti-CCSP Ab, and Deanna Penney, Melanie Majurie, Michele Timko, Janet Pan, and Victoria Mai for their technical assistance.

Disclosures

The authors have no financial conflicts of interest.

References

1. Suzuki, T., C. W. Chow, and G. P. Downey. 2008. Role of innate immune cells and their products in lung immunopathology. *Int. J. Biochem. Cell Biol.* 40: 1348–1361.
2. Bartlett, J. A., A. J. Fischer, and P. B. McCray, Jr. 2008. Innate immune functions of the airway epithelium. *Contrib. Microbiol.* 15: 147–163.
3. Kantari, C., M. Pederzoli-Ribeil, and V. Witko-Sarsat. 2008. The role of neutrophils and monocytes in innate immunity. *Contrib. Microbiol.* 15: 118–146.
4. Marriott, H. M., and D. H. Dockrell. 2007. The role of the macrophage in lung disease mediated by bacteria. *Exp. Lung Res.* 33: 493–505.

5. Parks, W. C., C. L. Wilson, and Y. S. Lopez-Boado. 2004. Matrix metalloproteinases as modulators of inflammation and innate immunity. *Nat. Rev. Immunol.* 4: 617–629.
6. Manicone, A. M., and J. K. McGuire. 2008. Matrix metalloproteinases as modulators of inflammation. *Semin. Cell Dev. Biol.* 19: 34–41.
7. Greenlee, K. J., D. B. Corry, D. A. Engler, R. K. Matsunami, P. Tessier, R. G. Cook, Z. Werb, and F. Kheradmand. 2006. Proteomic identification of in vivo substrates for matrix metalloproteinases 2 and 9 reveals a mechanism for resolution of inflammation. *J. Immunol.* 177: 7312–7321.
8. Corry, D. B., K. Rishi, J. Kanellis, A. Kiss, L. Z. Song Lz, J. Xu, L. Feng, Z. Werb, and F. Kheradmand. 2002. Decreased allergic lung inflammatory cell egression and increased susceptibility to asphyxiation in MMP2-deficiency. *Nat. Immunol.* 3: 347–353.
9. Li, Q., P. W. Park, C. L. Wilson, and W. C. Parks. 2002. Matrilysin shedding of syndecan-1 regulates chemokine mobilization and transepithelial efflux of neutrophils in acute lung injury. *Cell* 111: 635–646.
10. Cataldo, D. D., K. G. Tournoy, K. Vermaelen, C. Munaut, J. M. Foidart, R. Louis, A. Noel, and R. A. Pauwels. 2002. Matrix metalloproteinase-9 deficiency impairs cellular infiltration and bronchial hyperresponsiveness during allergen-induced airway inflammation. *Am. J. Pathol.* 161: 491–498.
11. Haro, H., H. C. Crawford, B. Fingleton, J. R. MacDougall, K. Shinomiya, D. M. Spengler, and L. M. Matrisian. 2000. Matrix metalloproteinase-3-dependent generation of a macrophage chemoattractant in a model of herniated disc resorption. *J. Clin. Invest.* 105: 133–141.
12. Haro, H., H. C. Crawford, B. Fingleton, K. Shinomiya, D. M. Spengler, and L. M. Matrisian. 2000. Matrix metalloproteinase-7-dependent release of tumor necrosis factor-α in a model of herniated disc resorption. *J. Clin. Invest.* 105: 143–150.
13. Hautamaki, R. D., D. K. Kobayashi, R. M. Senior, and S. D. Shapiro. 1997. Requirement for macrophage elastase for cigarette smoke-induced emphysema in mice. *Science* 277: 2002–2004.
14. Van Den Steen, P. E., A. Wuyts, S. J. Husson, P. Proost, J. Van Damme, and G. Opdenakker. 2003. Gelatinase B/MMP-9 and neutrophil collagenase/MMP-8 process the chemokines human GCP-2/CXCL6, ENA-78/CXCL5 and mouse GCP-2/LIX and modulate their physiological activities. *Eur. J. Biochem.* 270: 3739–3749.
15. Corry, D. B., A. Kiss, L. Z. Song, L. Song, J. Xu, S. H. Lee, Z. Werb, and F. Kheradmand. 2004. Overlapping and independent contributions of MMP2 and MMP9 to lung allergic inflammatory cell egression through decreased CC chemokines. *FASEB J.* 18: 995–997.
16. Lohi, J., C. L. Wilson, J. D. Roby, and W. C. Parks. 2001. Epilysin, a novel human matrix metalloproteinase (MMP-28) expressed in testis and keratinocytes and in response to injury. *J. Biol. Chem.* 276: 10134–10144.
17. Illman, S. A., J. Lohi, and J. Keski-Oja. 2008. Epilysin (MMP-28): structure, expression and potential functions. *Exp. Dermatol.* 17: 897–907.
18. Illman, S. A., J. Keski-Oja, W. C. Parks, and J. Lohi. 2003. The mouse matrix metalloproteinase, epilysin (MMP-28), is alternatively spliced and processed by a furin-like proprotein convertase. *Biochem. J.* 375: 191–197.
19. Li, Q. L., S. A. Illman, H. M. Wang, D. L. Liu, J. Lohi, and C. Zhu. 2003. Matrix metalloproteinase-28 transcript and protein are expressed in rhesus monkey placenta during early pregnancy. *Mol. Hum. Reprod.* 9: 205–211.
20. Illman, S. A., J. Keski-Oja, and J. Lohi. 2001. Promoter characterization of the human and mouse epilysin (MMP-28) genes. *Gene* 275: 185–194.
21. Skerrett, S. J., C. B. Wilson, H. D. Liggitt, and A. M. Hajjar. 2007. Redundant Toll-like receptor signaling in the pulmonary host response to *Pseudomonas aeruginosa*. *Am. J. Physiol.* 292: L312–L322.
22. Van Rooijen, N., and A. Sanders. 1994. Liposome mediated depletion of macrophages: mechanism of action, preparation of liposomes and applications. *J. Immunol. Methods* 174: 83–93.
23. Betsuyaku, T., G. L. Griffin, M. A. Watson, and R. M. Senior. 2001. Laser capture microdissection and real-time reverse transcriptase/polymerase chain reaction of bronchiolar epithelium after bleomycin. *Am. J. Respir. Cell Mol. Biol.* 25: 278–284.
24. Betsuyaku, T., and R. M. Senior. 2004. Laser capture microdissection and mRNA characterization of mouse airway epithelium: methodological considerations. *Micron* 35: 229–234.
25. Dunsmore, S. E., U. K. Saarialho-Kere, J. D. Roby, C. L. Wilson, L. M. Matrisian, H. G. Welgus, and W. C. Parks. 1998. Matrilysin expression and function in airway epithelium. *J. Clin. Invest.* 102: 1321–1331.
26. López-Boado, Y. S., C. L. Wilson, and W. C. Parks. 2001. Regulation of matrilysin expression in airway epithelial cells by *Pseudomonas aeruginosa* flagellin. *J. Biol. Chem.* 276: 41417–41423.
27. López-Boado, Y. S., C. L. Wilson, L. V. Hooper, J. I. Gordon, S. J. Hultgren, and W. C. Parks. 2000. Bacterial exposure induces and activates matrilysin in mucosal epithelial cells. *J. Cell Biol.* 148: 1305–1315.
28. Kassim, S. Y., S. A. Gharib, B. H. Mecham, T. P. Birkland, W. C. Parks, and J. K. McGuire. 2007. Individual matrix metalloproteinases control distinct transcriptional responses in airway epithelial cells infected with *Pseudomonas aeruginosa*. *Infect. Immun.* 75: 5640–5650.
29. Raivich, G., and R. Banati. 2004. Brain microglia and blood-derived macrophages: molecular profiles and functional roles in multiple sclerosis and animal models of autoimmune demyelinating disease. *Brain Res. Brain Res. Rev.* 46: 261–281.
30. Kooguchi, K., S. Hashimoto, A. Kobayashi, Y. Kitamura, I. Kudoh, J. Wiener-Kronish, and T. Sawa. 1998. Role of alveolar macrophages in initiation and regulation of inflammation in *Pseudomonas aeruginosa* pneumonia. *Infect. Immun.* 66: 3164–3169.
31. van Rooijen, N., and E. van Kesteren-Hendrikx. 2002. Clodronate liposomes: perspectives in research and therapeutics. *J. Liposome Res.* 12: 81–94.
32. van Rooijen, N., and E. van Kesteren-Hendrikx. 2003. "In vivo" depletion of macrophages by liposome-mediated "suicide". *Methods Enzymol.* 373: 3–16.
33. Schonbeck, U., F. Mach, and P. Libby. 1998. Generation of biologically active IL-1β by matrix metalloproteinases: a novel caspase-1-independent pathway of IL-1β processing. *J. Immunol.* 161: 3340–3346.
34. Gearing, A. J., P. Beckett, M. Christodoulou, M. Churchill, J. M. Clements, M. Crimmin, A. H. Davidson, A. H. Drummond, W. A. Galloway, R. Gilbert, et al. 1995. Matrix metalloproteinases and processing of pro-TNF-α. *J. Leukocyte Biol.* 57: 774–777.
35. Churg, A., R. D. Wang, H. Tai, X. Wang, C. Xie, J. Dai, S. D. Shapiro, and J. L. Wright. 2003. Macrophage metalloelastase mediates acute cigarette smoke-induced inflammation via tumor necrosis factor-α release. *Am. J. Respir. Crit. Care Med.* 167: 1083–1089.
36. Van den Steen, P. E., P. Proost, A. Wuyts, J. Van Damme, and G. Opdenakker. 2000. Neutrophil gelatinase B potentiates interleukin-8 tenfold by aminoterminal processing, whereas it degrades CTAP-III, PF-4, and GRO-α and leaves RANTES and MCP-2 intact. *Blood* 96: 2673–2681.
37. McQuibban, G. A., J. H. Gong, E. M. Tam, C. A. McCulloch, I. Clark-Lewis, and C. M. Overall. 2000. Inflammation dampened by gelatinase A cleavage of monocyte chemoattractant protein-3. *Science* 289: 1202–1206.
38. McQuibban, G. A., J. H. Gong, J. P. Wong, J. L. Wallace, I. Clark-Lewis, and C. M. Overall. 2002. Matrix metalloproteinase processing of monocyte chemoattractant proteins generates CC chemokine receptor antagonists with anti-inflammatory properties in vivo. *Blood* 100: 1160–1167.
39. Weathington, N. M., A. H. van Houwelingen, B. D. Noerager, P. L. Jackson, A. D. Kraneveld, F. S. Galin, G. Folkerts, F. P. Nijkamp, and J. E. Blalock. 2006. A novel peptide CXCR ligand derived from extracellular matrix degradation during airway inflammation. *Nat. Med.* 12: 317–323.
40. Maus, U., K. von Grote, W. A. Kuziel, M. Mack, E. J. Miller, J. Cihak, M. Stangassinger, R. Maus, D. Schlondorff, W. Seeger, and J. Lohmeyer. 2002. The role of CC chemokine receptor 2 in alveolar monocyte and neutrophil immigration in intact mice. *Am. J. Respir. Crit. Care Med.* 166: 268–273.
41. Kuziel, W. A., S. J. Morgan, T. C. Dawson, S. Griffin, O. Smithies, K. Ley, and N. Maeda. 1997. Severe reduction in leukocyte adhesion and monocyte extravasation in mice deficient in CC chemokine receptor 2. *Proc. Natl. Acad. Sci. USA* 94: 12053–12058.
42. Janatpour, M. J., S. Hudak, M. Sathe, J. D. Sedgwick, and L. M. McEvoy. 2001. Tumor necrosis factor-dependent segmental control of MIG expression by high endothelial venules in inflamed lymph nodes regulates monocyte recruitment. *J. Exp. Med.* 194: 1375–1384.
43. Mack, M., J. Cihak, C. Simonis, B. Luckow, A. E. Proudfoot, J. Plachy, H. Bruhl, M. Frink, H. J. Anders, V. Vielhauer, et al. 2001. Expression and characterization of the chemokine receptors CCR2 and CCR5 in mice. *J. Immunol.* 166: 4697–4704.
44. Rosseau, S., J. Selhorst, K. Wiechmann, K. Leissner, U. Maus, K. Mayer, F. Grimminger, W. Seeger, and J. Lohmeyer. 2000. Monocyte migration through the alveolar epithelial barrier: adhesion molecule mechanisms and impact of chemokines. *J. Immunol.* 164: 427–435.
45. Spertini, O., F. W. Luscinskas, M. A. Gimbrone, Jr., and T. F. Tedder. 1992. Monocyte attachment to activated human vascular endothelium in vitro is mediated by leukocyte adhesion molecule-1 (L-selectin) under nonstatic conditions. *J. Exp. Med.* 175: 1789–1792.
46. Meerschaert, J., and M. B. Furie. 1994. Monocytes use either CD11/CD18 or VLA-4 to migrate across human endothelium in vitro. *J. Immunol.* 152: 1915–1926.
47. Meerschaert, J., and M. B. Furie. 1995. The adhesion molecules used by monocytes for migration across endothelium include CD11a/CD18, CD11b/CD18, and VLA-4 on monocytes and ICAM-1, VCAM-1, and other ligands on endothelium. *J. Immunol.* 154: 4099–4112.
48. Maus, U., J. Huwe, L. Ermert, M. Ermert, W. Seeger, and J. Lohmeyer. 2002. Molecular pathways of monocyte emigration into the alveolar air space of intact mice. *Am. J. Respir. Crit. Care Med.* 165: 95–100.
49. Werner, S. R., A. L. Mescher, A. W. Neff, M. W. King, S. Chaturvedi, K. L. Duffin, M. W. Harty, and R. C. Smith. 2007. Neural MMP-28 expression precedes myelination during development and peripheral nerve repair. *Dev. Dyn.* 236: 2852–2864.
50. Cheung, D. O., K. Halsey, and D. P. Speert. 2000. Role of pulmonary alveolar macrophages in defense of the lung against *Pseudomonas aeruginosa*. *Infect. Immun.* 68: 4585–4592.
51. McClellan, S. A., X. Huang, R. P. Barrett, N. van Rooijen, and L. D. Hazlett. 2003. Macrophages restrict *Pseudomonas aeruginosa* growth, regulate polymorphonuclear neutrophil influx, and balance pro- and anti-inflammatory cytokines in BALB/c mice. *J. Immunol.* 170:5219–5227.